Impact of 3D groundwater dynamics on heat events in historical regional climate simulations over Europe

Liubov Poshyvailo-Strube[1,2], Niklas Wagner[1,2], Klaus Goergen[1,2], Carina Furusho-Percot[3], Carl Hartick[1,2,4], and Stefan Kollet[1,2]

[1]Institute of Bio- and Geosciences: Agrosphere (IBG-3), Forschungszentrum Jülich GmbH, Jülich, Germany
[2]Centre for High-Performance Scientific Computing in Terrestrial Systems (HPSC TerrSys), Geoverbund ABC/J, Jülich, Germany
[3]National Research Institute for Agriculture, Food and Environment (INRAE), Avignon, France
[4]Jülich Supercomputing Centre (JSC), Forschungszentrum Jülich GmbH, Jülich, Germany

Correspondence: Liubov Poshyvailo-Strube (l.poshyvailo@fz-juelich.de)

Abstract. The representation of groundwater processes is simplified in most regional climate models (RCMs), potentially leading to biases in simulated heat waves. This paper introduces a unique dataset from the regional Terrestrial Systems Modelling Platform (TSMP) forced by Max Planck Institute Earth System Model at Low Resolution (MPI-ESM-LR) boundary conditions for a historical time span in the context of dynamical downscaling of global climate models (GCMs) for climate change studies. TSMP explicitly represents 3D subsurface and groundwater dynamics together with overland flow, closing the water and energy cycle from the bedrock to the top of the atmosphere. By comparing summer heat events statistics (i.e. a series of consecutive days with a near-surface temperature exceeding the 90th percentile of the reference period) from TSMP and those from GCM-RCM simulations with simplified groundwater dynamics from the Coordinated Regional Climate Downscaling Experiment (CORDEX) for the European domain, we aim to improve the understanding of how 3D groundwater dynamics affect regional heat events over Europe.

The analysis is carried out for 1976-2005 relative to the 1961-1990 period. While our results show that TSMP simulates heat events consistently with the CORDEX ensemble, there are some systematic differences that we attribute to the representation of groundwater in TSMP. Compared to the CORDEX ensemble, TSMP simulates lower means and lower interannual variability in the number of hot days (i.e., days with a near-surface temperature exceeding the 90th percentile of the reference period) on average over Europe. The decadal change in the number of hot days is also lower in TSMP than on average in the CORDEX ensemble. TSMP systematically simulates fewer heat waves (i.e., heat events lasting 6 days or more) compared to the CORDEX ensemble, moreover, they are less intense. Southern Europe is particularly sensitive to groundwater coupling, while Scandinavia is the least sensitive. Therefore, an explicit representation of groundwater dynamics in RCMs may be a key in reducing the bias in simulated duration and intensity of heat waves, especially in Southern Europe. The results emphasise the importance of groundwater coupling in long-term regional climate simulations and potential implications for climate change projections.

1 Introduction

Over the past decades, the number of heat waves has increased (e.g., Frich et al., 2002; Alexander et al., 2006; Christidis et al., 2015; Zhang et al., 2020). The years 2003, 2010, 2018, and 2022 were exceptionally hot in Europe, characterised by record-breaking near-surface air temperatures (e.g., Stott et al., 2004; Barriopedro et al., 2011; Liu et al., 2020; Dirmeyer et al., 2021; Yule et al., 2023). With projected climate change, the occurrence of heat waves will continue to increase (e.g., Russo et al., 2015; Myhre et al., 2019; Hari et al., 2020; Molina et al., 2020; Masson-Delmotte et al., 2021), leading to multiple negative socio-economic impacts (e.g., Bosello et al., 2007; Ciscar et al., 2011; Amengual et al., 2014; Yin et al., 2022).

The underlying hydrometeorological mechanisms of heat waves have been extensively studied (e.g., Lhotka and Kyselý, 2015; Horton et al., 2016; Liu et al., 2020). Heat waves are triggered by strong, persistent quasi-stationary large-scale high pressure systems associated with atmospheric blocking events, resulting in subsiding, adiabatically warming air masses, and clear skies allowing for high insolation (Tomczyk and Bednorz, 2016; Horton et al., 2016; Kautz et al., 2022). Atmospheric blocking events also impact winter and early spring precipitation in most parts of Europe and, in turn, affect soil moisture (e.g., Vautard et al., 2007; Ionita et al., 2020). The evolution of heat waves depends primarily on the synoptic weather patterns in combination with ambient soil moisture conditions, further altered by multiple land-atmosphere feedback processes (e.g., Fischer et al., 2007; Horton et al., 2016).

Many European summer heat waves were preceded by a deficiency of spring precipitation (Dirmeyer et al., 2021; Stegehuis et al., 2021; Hartick et al., 2021). Due to the soil moisture memory effect, the lack of precipitation in early spring causes negative soil moisture anomalies in early summer and leads to strong land-atmosphere coupling (a measure of the response of the atmosphere to anomalies in the land surface state) with a lower evaporation fraction. This reduces latent cooling and amplifies summer temperatures (e.g., Fischer et al., 2007; Miralles et al., 2012; Knist et al., 2017; Dirmeyer et al., 2021). Note that soil moisture memory is a phenomenon of persistence of wet or dry anomalies over a long period of time, from weeks to months, after the atmospheric conditions that caused them have passed; this allows to preserve the hydroclimatic conditions of the preceding months (e.g., Manabe and Delworth, 1990; Song et al., 2019). Thus, depending on soil moisture conditions, the soil moisture memory effect can contribute to either buffering negative droughts impacts and weakening a heat wave, or, conversely, delaying drought recovery and exacerbating the occurrence of a heat wave (e.g., Erdenebat and Tomonori, 2018; Martínez-de la Torre and Miguez-Macho, 2019). In addition to precipitation, soil moisture is strongly influenced by groundwater dynamics via vertical fluxes across the water table (capillary rise) and via horizontal fluxes through gravity-driven lateral transport within the saturated zone. Here, the water table depth dictates the intensity of shallow groundwater–soil moisture and evapotranspiration coupling (Kollet and Maxwell, 2008).

In the context of climate impact assessments, dynamical downscaling of global climate models (GCMs) with regional climate models (RCMs) is widely used to generate regional climate change scenario information (Vautard et al., 2013b; Mearns et al., 2015; Jacob et al., 2020). RCMs have been shown to provide added value to driving GCMs by better capturing small-scale processes (Giorgi and Gutowski, 2015; Torma et al., 2015; Prein et al., 2016; Iles et al., 2020; Rummukainen, 2016), but model biases (offset during the historical period against observations) and uncertainties in climate projections still remain

(Hawkins and Sutton, 2009; Lhotka et al., 2018; Sørland et al., 2018; Fernandez-Granja et al., 2021). In fact, many RCMs tend to overestimate the frequency, duration, and intensity of heat waves (Vautard et al., 2013a; Plavcová and Kyselý, 2016; Lhotka et al., 2018; Furusho-Percot et al., 2022).

The role of soil moisture in modelling heat waves is crucial (e.g., Seneviratne et al., 2006, 2010; Fischer et al., 2007), but due to the complexity of the feedbacks involved and related high computational cost, the explicit representation of hydrological processes is oversimplified or neglected in most RCMs. Commonly applied hydrology schemes are based on 1D-parameterizations in the vertical direction with runoff generation at the land surface and a gravity driven free drainage approach as the lower boundary condition; in such a parametrisation there is no lateral subsurface flow and only the 1D-Richards' equation is solved (e.g., Niu et al., 2007; Campoy et al., 2013). RCMs with a simplified representation of hydrological processes have difficulties in reliably reproducing the land surface energy flux partitioning and, consequently, near-surface air temperatures, leading to warm biases (Vautard et al., 2013a; Barlage et al., 2021; Furusho-Percot et al., 2022). Hydrological parameters tuning (e.g., Teuling et al., 2009; Bellprat et al., 2016) or developing new parameterizations of groundwater dynamics (e.g., Liang et al., 2003; Yeh and Eltahir, 2005; Schlemmer et al., 2018) have been shown to improve model results. A physically consistent description of hydrological processes in RCMs can be achieved by an explicit representation of 3D subsurface and groundwater hydrodynamics together with overland flow. Thereby accounting for the feedback loops over the terrestrial system (Maxwell et al., 2007), i.e., the closure of water and energy cycles from groundwater across the land surface to the top of the atmosphere, as for instance in the Terrestrial Systems Modelling Platform (TSMP) (e.g., Shrestha et al., 2014; Gasper et al., 2014), a regional climate system model.

Keune et al. (2016) demonstrated the link between groundwater dynamics and near-surface air temperature in an analysis of the August 2003 European heat wave from TSMP simulations nested within ERA-Interim reanalysis (Dee et al., 2011). The model was set up over the European domain of the Coordinated Regional Climate Downscaling Experiment (CORDEX) (Gutowski et al., 2016; Jacob et al., 2020) with two different groundwater configurations: (i) simplified 1D free drainage approach and (ii) 3D physics-based variably saturated groundwater dynamics. The study clearly showed the impact of groundwater dynamics on the land surface water and energy balance: latent heat fluxes were higher and maximum temperatures were lower, especially in areas with shallow water table depth, in the 3D configuration compared to the simplified 1D free drainage approach. Keune et al. (2016) suggest that the 3D groundwater dynamics in TSMP alleviate the evolution of a single heat wave due to weaker land-atmosphere feedbacks compared to the simplified 1D free drainage approach, at least during the investigated European heat wave of summer 2003.

Therefore, compared to the 1D approach, the 3D groundwater dynamics in TSMP leads to regionally shallow groundwater levels, causing wetter soils, and a reduction in the Bowen ratio (i.e., ratio between sensible heat flux to latent heat flux) due to an increase in surface latent heat flux and a decrease in surface sensible heat flux, that leads to increased evapotranspiration (Maxwell and Condon, 2016). Such an increase in a latent heat flux also causes moistening of the lower atmosphere and increases downward longwave radiation due to the greenhouse effect of water vapor, on the other hand, it cools the surface and reduces outgoing surface longwave radiation. In addition, increased evapotranspiration may cause moist convection or rainfall, which further affects soil moisture (Eltahir, 1998; Pal and Eltahir, 2001; Yang et al., 2018). In its turn, the simplified repre-

sentation of groundwater dynamics with the 1D free drainage approach leads to the opposite effect, namely an overestimation of the land surface-atmosphere coupling, i.e., deeper groundwater levels cause drier soils, an increase in the Bowen ratio, a decrease in cloud cover and enhancement of net solar radiation and, as a result, higher near-surface temperatures, which in turn further reduces soil moisture (e.g., Vogel et al., 2018; Hartick et al., 2022). The ability of groundwater to decrease warm summer biases and moderate maximum air temperatures during a single seasonal heat wave in RCM simulations was also discussed in Barlage et al. (2015, 2021) and Mu et al. (2022).

Further studies were carried out to understand whether the observed differences in simulated near-surface temperature due to differences in groundwater configuration persist over a long time period, and how this manifests itself for heat waves in the CORDEX realm for the European domain. Furusho-Percot et al. (2019) showed that TSMP evaluation run (1996–2018) forced by the ERA-Interim reanalysis is able to capture climate system dynamics and the succession of warm and cold seasons on the regional scale for PRUDENCE regions (Christensen and Christensen, 2007) consistently with E-OBS observations (Cornes et al., 2018). Furusho-Percot et al. (2022) demonstrated that TSMP multiannual simulations exhibit lower deviations of summer heat wave indices from the E-OBS observational dataset, compared to ERA-Interim driven RCM evaluation simulations of the CORDEX experiment, which tend to simulate too persistent heat waves. This particular behaviour of TSMP is attributed to its improved hydrology. The improved capacity to sustain soil moisture translates into more reliable latent heat flux and evapotranspiration, which in turn leads to a decrease in heat wave intensity, its spatial extent, and the number of days with anomalously high near-surface temperatures. An important question still remains: how will these findings be reflected in long-term regional climate simulations?

In this paper, we present a unique dataset from the regional climate system model TSMP forced by the Max Planck Institute Earth System Model at Low Resolution, MPI-ESM-LR (Giorgetta et al., 2013) historical boundary conditions in the context of regional long-term climate simulations and dynamical GCM-RCM downscaling for climate change studies. We interrogate the statistics of the characteristics (frequency, duration, intensity) of heat events for the summer seasons of 1976-2005 with respect to the reference period 1961-1990 by comparing TSMP results with the CORDEX multi-model RCM ensemble driven by GCM control simulations of phase five of the Coupled Model Intercomparison Project (CMIP5) (Taylor et al., 2012), to understand the influence of 3D groundwater dynamics on simulated heat events for historical regional climate simulations and potential consequences for ensuing climate change projections. While the 1996-2018 TSMP evaluation runs nested within ERA-Interim reanalysis were examined for heat wave statistics by Furusho-Percot et al. (2022), long-term historical climate simulations of TSMP forced by GCM over CORDEX European domain have not been previously presented. Thus, this is the first downscaled regional historical climate simulation over Europe from groundwater across the land surface to the top of the atmosphere, analysed for summer heat events.

In Sec. 2, we describe the TSMP modelling platform and its setup, the ensemble of CORDEX GCM-RCM climate change scenario control runs and the methodology of heat events analysis are also presented here. In Sect. 3, we examine the new TSMP dataset for consistency with the CORDEX ensemble and present results on the impact of 3D groundwater dynamics on simulated heat events in regional historical climate simulations. Section 4 provides a summary and overall conclusions.

2 Methods

2.1 TSMP

TSMP is a scale-consistent, highly modular, fully integrated soil-vegetation-atmosphere modelling system (e.g., Shrestha et al., 2014; Gasper et al., 2014). TSMP consists of three component models: the atmospheric COnsortium for Small Scale Modelling (COSMO) model version 5.01, the Community Land Model (CLM) version 3.5, and the hydrological model ParFlow version 3.2. The component models are externally coupled via the Ocean Atmosphere Sea Ice Soil (OASIS) version 3.0 Model Coupling Toolkit (MCT) (e.g., Valcke, 2013), which enables closure of the terrestrial water and energy cycles from the bedrock to the top of the atmosphere.

COSMO is a non-hydrostatic limited-area atmospheric model (e.g., Baldauf et al., 2011). It is based on the primitive thermo-hydrodynamical Euler equations formulated in rotated geographical coordinates and generalized terrain-following height coordinates, describing compressible flow in a moist atmosphere. COSMO parameterization schemes cover various physical processes, such as radiation, cloud microphysics, deep convection, etc. The boundary conditions are provided by a coarse grid model, whereas the lower boundary conditions (e.g., surface albedo, energy fluxes, surface temperature, surface humidity) are provided by CLM.

CLM is a biogeophysical model of the land surface (e.g., Oleson et al., 2004, 2008). It simulates land-atmosphere exchanges in response to atmospheric forcings. CLM consist of four components that describe biogeophysics, hydrologic cycle, biogeochemistry, and dynamic vegetation. In TSMP, CLM receives short-wave radiation, wind speeds, barometric pressure, precipitation, near-surface temperature, and specific humidity from COSMO. In turn, CLM sends infiltration and evapotranspiration fluxes for each soil layer of ParFlow.

ParFlow is a hydrological model that simulates variably saturated three-dimensional subsurface hydrodynamics using Richards equation integrated with shallow overland flow based on a kinematic wave approximation (e.g., Maxwell and Miller, 2005; Kollet and Maxwell, 2006; Kuffour et al., 2020). ParFlow allows 3D-redistribution of subsurface water in a continuum approach. In TSMP, ParFlow replaces the hydrologic functionality of CLM.

2.2 Model setup

TSMP simulations are conducted for the historical time period from December 1949 to the end of 2005 over the European domain according to the CORDEX simulation protocol (e.g., Gutowski et al., 2016) using rotated latitude-longitude model grid with a horizontal resolution of 0.11° (EUR-11) or about 12.5 km. Note that these model runs are the first CORDEX climate change control simulations over Europe with explicit representation of 3D groundwater. The COSMO configuration used in this TSMP setup resembles that of the COSMO model in CLimate Mode (CCLM) (e.g., Rockel et al., 2008). COSMO extends vertically up to 22 km, divided into 50 levels. CLM has 10 soil layers with a total depth of 3 m. These layers coincide with the 10 top layers of ParFlow, which has 5 additional layers that increase in thickness to a total depth of 57 m. The time step for ParFlow and CLM is 900 sec, for COSMO it is 75 sec. The coupling time step between TSMP component models is 900 sec.

For CLM, plant functional types (PFT) are taken from the Moderate Resolution Imaging Spectroradiometer (MODIS) dataset (Friedl et al., 2002). Leaf area index, stem area index, and the monthly bottom and top heights of each PFT are calculated based on the global CLM surface dataset (Oleson et al., 2008). Compared to the previous studies of Furusho-Percot et al. (2019, 2022); Hartick et al. (2021), where soil parameters were assumed to be vertically homogenous in ParFlow, in this work we have improved the subsurface hydrogeology, which is described below. Static input fields (i.e., soil color, percentage clay, percentage sand, dominant land use type, dominant soil types in the top layers, dominant soil types in the bottom layers and subsurface aquifer and bedrock bottom layers) are derived from MODIS, Food and Agriculture Organization soil database (FAO, 1988), pan-European River and Catchment Database (Vogt et al., 2007), International Hydrogeological map of Europe (IHME) (Duscher et al., 2015) and the GLobal HYdrogeology MaPS (GLHYMPS) (Gleeson et al., 2014). The pan-European River and Catchment Database serves in ParFlow as a proxy for the alluvial aquifer system, with the assumption that alluvial aquifers lie underneath or in proximity of existing rivers.

Forcing data for the TSMP atmospheric component model, i.e., for COSMO, are provided by the Max-Planck Institute's MPI-ESM-LR r1i1p1 CMIP5 GCM with a resolution of T63L47 (Giorgetta et al., 2013). CLM and ParFlow are initialised (i.e., land surface, subsurface hydrology, and energy states) with the moisture conditions of the 1st of December 2011 from the previous evaluation run driven by ERA-Interim reanalysis (Furusho-Percot et al., 2019). In the analysis, we discard the first 10 years of TSMP simulations due to hydrodynamic spin-up.

2.3 CORDEX ensemble

The selected CORDEX ensemble members of the multi-physics RCMs with EUR-11 horizontal resolution driven by different CMIP5 GCMs (r1i1p1 ensemble members) is used in conjunction with the coupled TSMP modelling platform to study the characteristics of summer heat events. Note that CMIP5 GCM historical control simulations are performed under observed natural and anthropogenic forcing (Taylor et al., 2012). Suggestions and limitations of multi-model GCM-RCM ensembles were previously discussed in, for example, Déqué et al. (2007); Kendon et al. (2010); Fernández et al. (2019); Vautard et al. (2021). In this study, based on availability, the following models are considered, identified by their institutions: CLMcom (CCLM4-8-17 forced by MPI-ESM-LR and CNRM-CM5), CLMcom-ETH (COSMO-crCLIM forced by MPI-ESM-LR, CNRM-CM5, and NCC-NorESM1-M), MPI-CSC (REMO2009 driven by MPI-ESM-LR), GERICS (REMO2015 forced by NCC-NorESM1-M, NOAA-GFDL-ESM2G, and IPSL-CM5A-LR); see Table 1. The considered CORDEX multi-model ensemble includes two main groups of RCMs, namely COSMO and REMO, driven by 5 different GCMs, for a total of 10 different GCM-RCM pairs. The CORDEX RCM most compatible with TSMP is CCLM4-8-17, where the largest differences arise from the lower boundary condition in COSMO: in TSMP, the lower boundary condition for COSMO accounts for groundwater feedbacks due to the coupling with the land surface model CLM and the hydrologic model ParFlow, unlike CCLM4-8-17, where soil processes are modelled with the TERRA-ML soil-vegetation land surface model (Grasselt et al., 2008; Doms et al., 2013). All members of the ensemble, except for TSMP, include simplified representations of subsurface hydrodynamics.

Note that the ensemble of CORDEX climate change scenario RCM control runs is not intended for direct comparison between individual models, as it includes different RCMs in combination with different driving GCMs. Therefore, due to

Table 1. The multi-model ensemble of GCM-RCM climate change scenario control runs.

GCM-RCM	MPI-ESM-LR *(Giorgetta et al., 2013)*	CNRM-CM5 *(Voldoire et al., 2013)*	NCC-NORESM1-M *(Bentsen et al., 2013)*	NOAA-GFDL-ESM2G *(Dunne et al., 2012)*	IPSL-CM5A-LR *(Dufresne et al., 2013)*
TSMP *(Shrestha et al., 2014)*	X				
CCLM4-8-17 *(Rockel et al., 2008)*	X	X			
COSMO-crCLIM *(Pothapakula et al., 2020)*	X	X	X		
REMO2009 *(Jacob and Podzun, 1997)*	X				
REMO2015			X	X	X

connections of various factors (e.g., model setup, conceptual and structural model uncertainties, different physical parameterizations, internal variability, representation of subsurface-land-atmosphere interactions, lower and lateral atmospheric GCM boundary conditions, etc.) in addition to groundwater coupling, it is challenging to reveal the exact cause-and-effect relationships between the explicit groundwater representation and simulated hot days, as well as the associated characteristics of heat events, in the multi-model CORDEX ensemble. However, the consideration of an extended period, e.g., 30 years, allows to draw statistical conclusions. This study aims to investigate whether the new dataset from TSMP driven by MPI-ESM-LR is consistent with the CORDEX ensemble and, in particular, to gain insight into the role of groundwater for long-term climate simulations from the statistical analysis of heat events over Europe.

2.4 Analysis of heat events

There is no universally accepted method for defining heat events, but the most commonly used approach is built on a percentile temperature threshold (e.g., Zhang et al., 2005, 2011; Sulikowska and Wypych, 2020). Note that although the focus is on temperature-based diagnostics, it is often ambiguous or inconsistent, describing heat events only partially (Perkins and Alexander, 2013).

In this study, we define a hot day as a day with a daily mean temperature above the local 90th percentile of the reference period. We calculate the 90th percentile for every summer day and for each EUR-11 grid point of the CORDEX European domain from a consecutive 5-day moving window centered on that calendar day from the 30-year reference period between 1961 and 1990. The first occurrence of a hot day determines the start of a heat event. A series of hot days constitutes a heat event, highlighted in dark red in Fig. 1. A heat event is interrupted if the mean daily temperature drops below the 90th percentile-based threshold.

A heat event can be characterised by its duration, intensity, and frequency (e.g., Horton et al., 2016). A heat event duration is the number of consecutive days over which the heat event lasts. If a heat event lasts long enough, it can be classified as a heat wave. Similar to Fischer and Schär (2010), we consider a heat wave as a spell of at least six consecutive days with mean daily 2 m air temperatures above the local 90th percentile of the reference 1961-1990 period. See Fig. 1 for the explanation of a

heat wave detection. Therefore, we consistently use the terminology “hot day”, “heat event”, and “heat wave” throughout this analysis.

Note that the total number of hot days during the investigated period corresponds to the TG90p heat index from the joint CCl/CLIVAR/JCOMM Expert Team on Climate Change Detection and Indices (ETCCDI) (e.g., Zhang et al., 2011). TG90p describes the number of days with $TG_{ij} > TG_{in}90$, where TG_{ij} is the mean daily temperature on day i of the investigated period j and $TG_{in}90$ is the 90th percentile calculated for day i from a 30-year reference period n.

A heat event intensity is the maximum of the difference between the mean daily temperature and the 90th percentile of the reference 1961-1990 period within a single heat event (e.g., Vautard et al., 2013a). Intensity represents the severity of a heat event (see Fig. 1). Adopting the definition from the heat wave duration index (Frich et al., 2002), we classify a heat wave as intense if it exceeds 5 K. Some studies group heat waves according to their intensity as low, severe, or extreme (e.g., Nairn and Fawcett, 2014).

A frequency of heat events of a certain type (e.g., of a certain duration or intensity) over the investigated period is the number of these heat events divided by the total number of all heat events that occurred during the period under study (e.g., Vautard

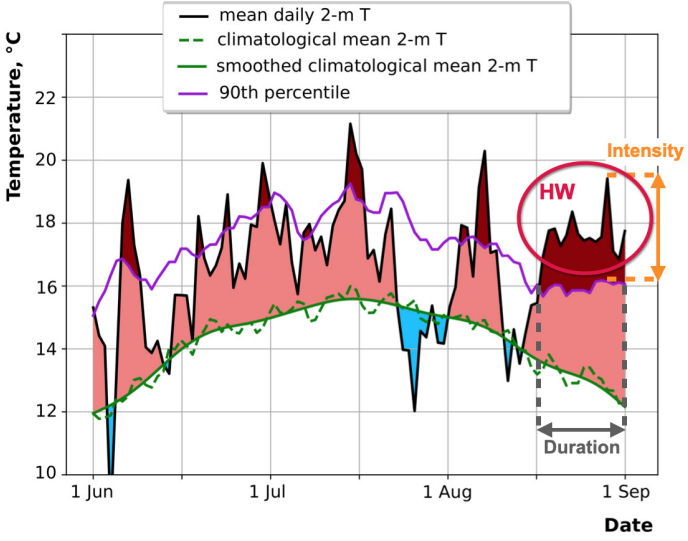

Heat event #	Start date	End date	Duration, days	Intensity, °C
1.	1.06	1.06	1	0,26
2.	6.06	9.06	4	2,71
3.	19.06	19.06	1	1,30
4.	24.06	24.06	1	1,07
5.	30.06	1.07	2	1,40
6.	7.07	7.08	2	0,41
7.	15.07	17.07	3	1,90
8.	3.08	4.08	2	0,63
9.	6.08	7.08	2	3,08
10.	**17.08**	**31.08**	**15**	**3,28**

Figure 1. Schematic of detection of a summer heat wave (HW). An example is given for June-July-August of 1972 for one grid point [250, 300] of the CORDEX European domain. Data taken from the TSMP simulations. The solid black line is the mean daily 2 m air temperature for the summer season of 1972. The dashed green line shows the climatological mean daily 2 m air temperature calculated from the reference period 1961-1990, and the solid green line is its smoothing with a Butterworth filter. The solid violet line represents the 90th percentile of the mean daily 2 m air temperature calculated from a 5-day window centered on each calendar day of the 1961-1990 reference period. The shaded light red colour indicates days with temperatures above the climatological mean, and the shaded dark red colour emphasizes days with temperatures above the 90th percentile, classified within the scope of this paper as “hot days”, “heat events”, or “heat waves”.

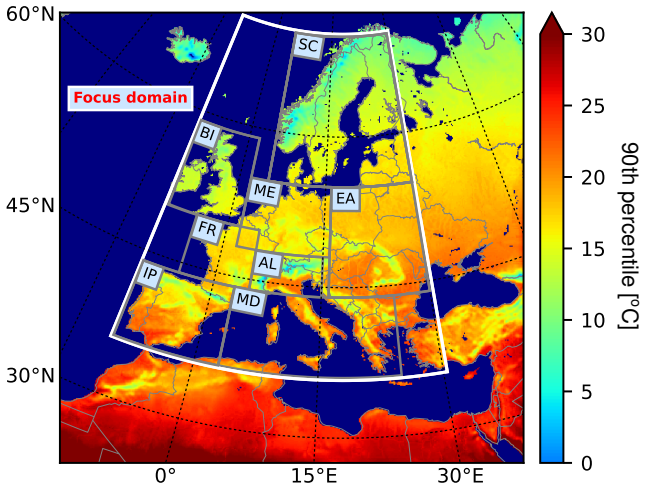

Figure 2. Summer mean 90th percentile of 2 m air temperatures in TSMP simulations. The 90th percentile is calculated from a consecutive 5-day moving window over the reference period 1961-1990. The white box indicates the focus domain for the analysis [10°W-30°E, 36°N-70°N]. PRUDENCE regions are shown with grey boxes: British Isles (BI), Iberian Peninsula (IP), France (FR), Mid-Europe (ME), Scandinavia (SC), Alps (AL), Mediterranean (MD) and Eastern Europe (EA).

et al., 2013a). For example, in Fig. 1, the frequency of heat events with 2 days duration is equal to the number of those heat events, i.e. 4 divided by the total number of all heat events, i.e. 10. The resulting frequency is 0.4 and indicates that 40% of all heat events have a duration of 2 days.

In this study, we examine heat events in Europe by assessing their characteristics as explained above, based on mean daily 2 m air temperatures on the native EUR-11 grid for TSMP simulations and the CORDEX ensemble of GCM-RCM climate change scenario control runs (see Table 1). The analysis is conducted in the focus domain covering the European continent [10°W-30°E, 36°N-70°N], as shown in Fig. 2, for the summer season of the 30-year period, from 1976 to 2005, with regard to the reference period 1961-1990 in each RCM. Note that we analyse only grid elements that belong to land.

3 Results

3.1 Hot days number

To assess the impact of groundwater dynamics on the interannual variability of the number of hot days during the summer season, we examine the occurrence of hot days in the focus domain in the TSMP simulations and the CORDEX ensemble from 1976 to 2005 with regard to the reference period 1961-1990. A comparison of the mean number of hot days averaged over the total number of land grid points in the focus domain, i.e., the mean seasonal TG90p index, suggests that the impact of groundwater coupling varies from year to year (Fig. 3). Here, the long-term soil moisture memory effects can play an important role, for example by increasing the probability of a subsurface water storage deficit in regions that have had a subsurface water

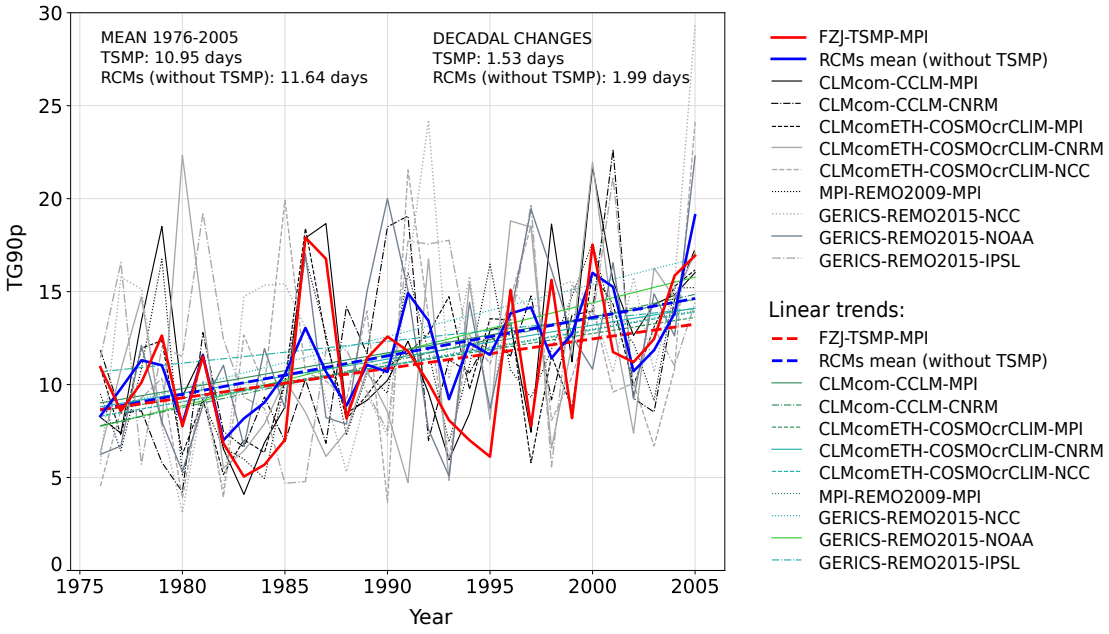

Figure 3. Time series of the mean TG90p index and its linear trends during the summer season in the focus domain during 1976-2005 with respect to the reference period 1961-1990, in the TSMP simulations and the CORDEX ensemble. Averaging of TG90p is performed over the total number of land grid points in the focus domain every sumer. The solid and dashed red lines show the mean TG90p and its linear trend from the TSMP simulations. The black and grey lines represent the mean TG90p index from the CORDEX ensemble and the green lines are their linear trends respectively. The TG90p index averaged over the multi-model CORDEX ensemble is shown with the solid blue line, and its linear trend is shown with the dashed blue line.

deficit in the previous year (e.g., Hartick et al., 2021), thereby influencing the occurrence of hot days (see description of the respective processes in Sec. 1). A positive linear trend in the mean TG90p index in the focus domain is observed in all considered RCMs (see Fig. 3). The decadal change of the mean TG90p index in the TSMP simulations is 1.53 days, whereas its value averaged over the multi-model CORDEX ensemble reaches up to 2 days.

A spatial distribution of the mean TG90p index and its variability as well as the decadal change, for 1976-2005 with respect to the reference period 1961-1990, are shown in Fig. 4-6. Note that the uncertainty in simulated near-surface temperature in summer is strongly controlled by the large-scale atmospheric circulation imposed by the GCM boundary conditions, with the largest impacts occurring in the southwestern PRUDENCE regions (e.g., Déqué et al., 2012; Evin et al., 2021). For this reason, the spatial pattern of the TG90p index in RCMs driven by the same GCMs show a rather similar behaviour. TSMP produces the smoothest spatial distribution of the mean TG90p index and its variability compared to the CORDEX ensemble (see standard deviations indicated in Fig. 4, 5), suggesting that an explicit representation of groundwater dynamics in RCMs may lead to more steady climate with respect to the interannual changes in the simulated number of hot days in summer. Details on the TG90p mean, variability, and decadal change averaged over the PRUDENCE regions and the focus domain, from the TSMP simulations and the CORDEX ensemble, are given in Appendix A.

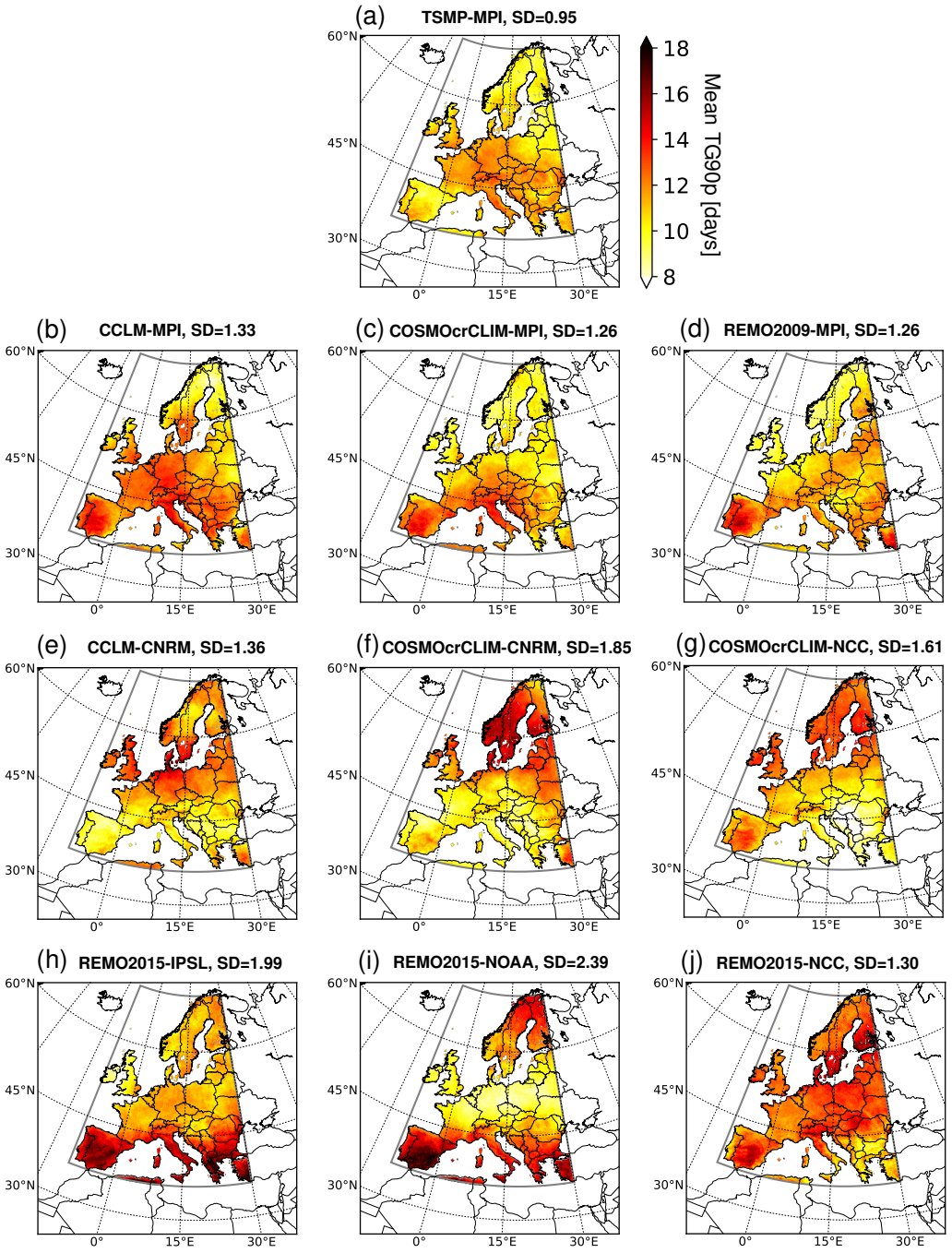

Figure 4. Spatial distribution of the mean TG90p index for the summer season averaged between 1976 and 2005 with respect to the reference period 1961-1990, in TSMP and the CORDEX ensemble. The standard deviation (SD) is indicated in every figure.

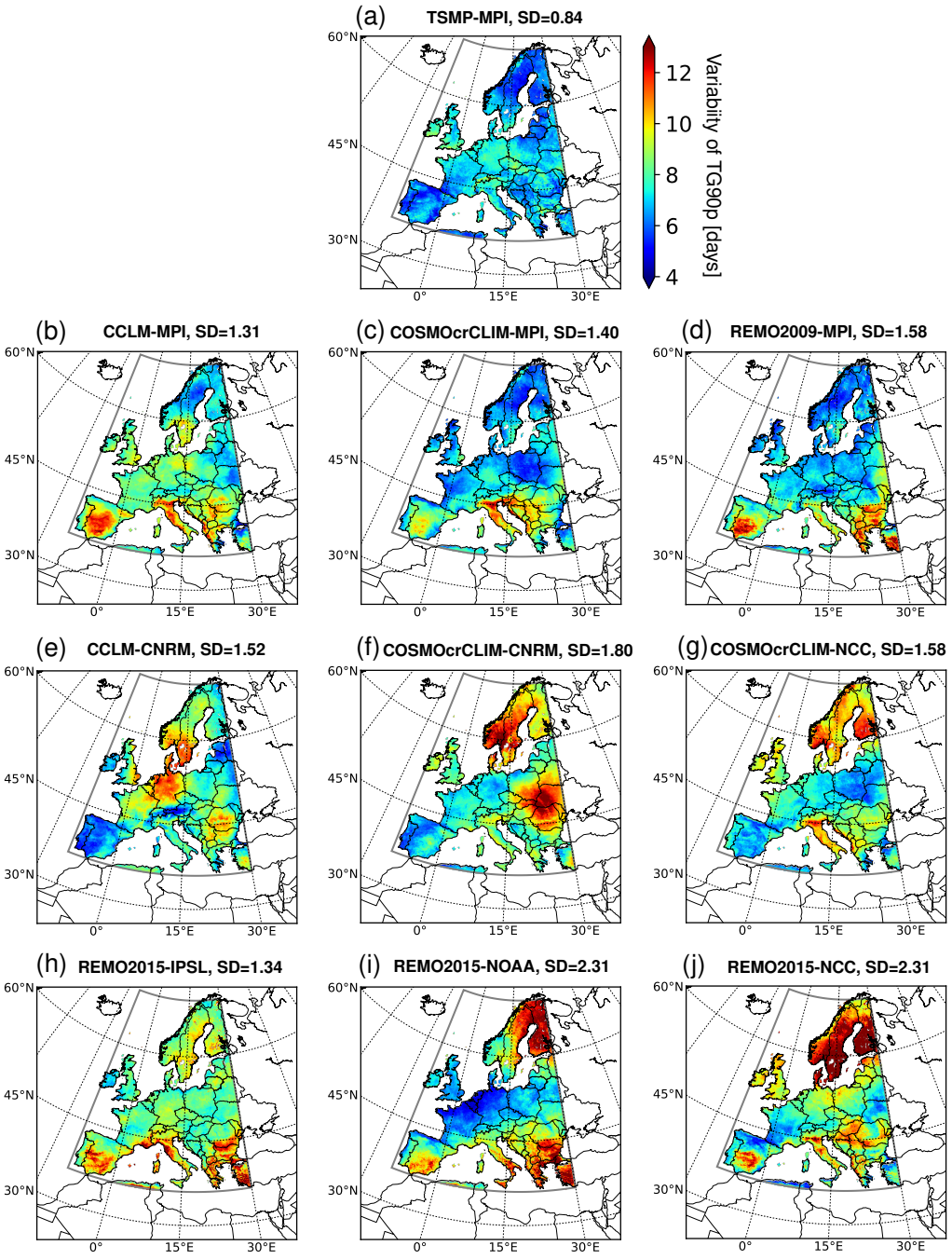

Figure 5. Variability of the TG90p index, calculated from the summer seasonal TG90p during 1976-2005 as the standard deviation at each land grid element, for TSMP and the CORDEX ensemble. The standard deviation (SD) of the spatial distribution of the TG90p variability is indicated in every figure.

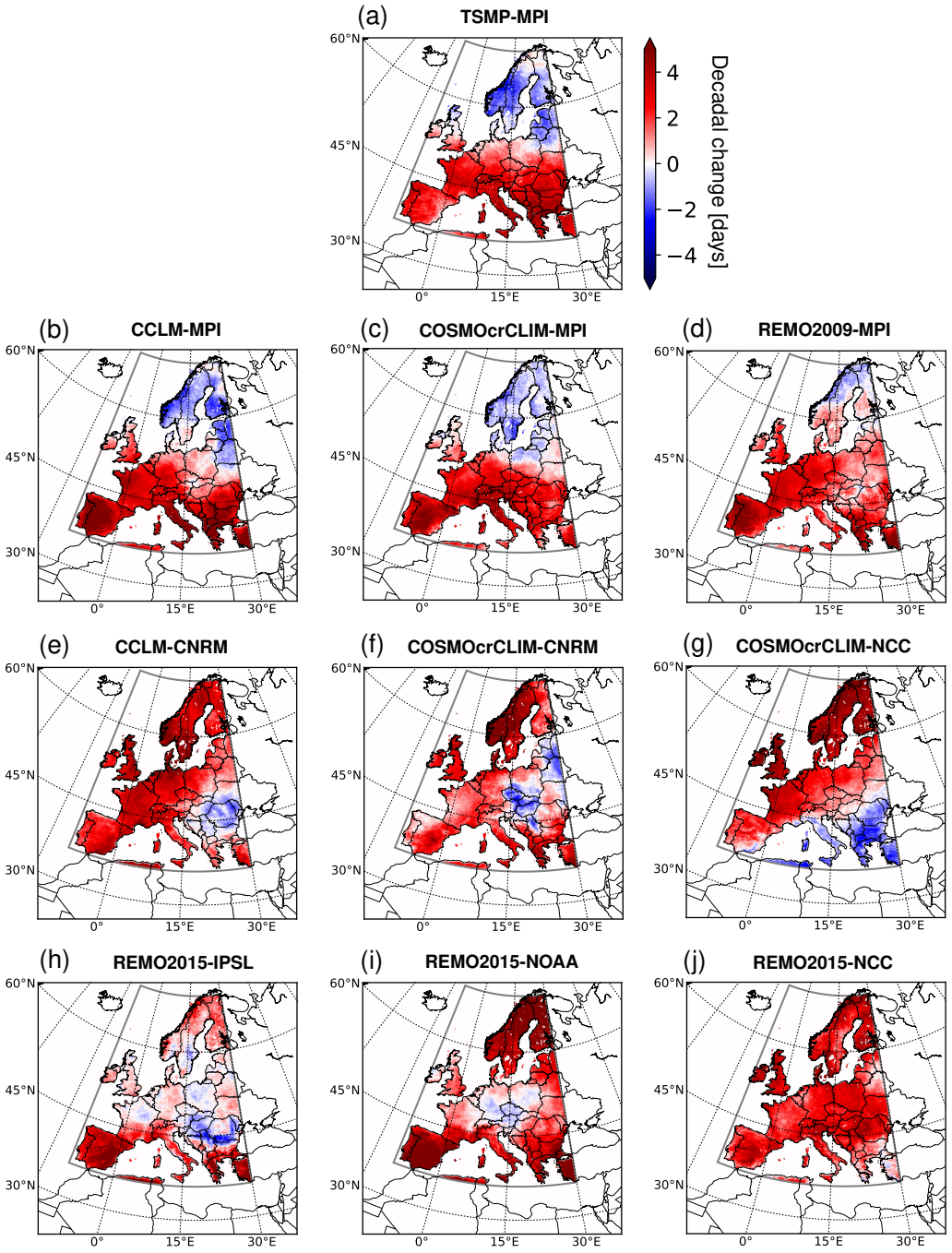

Figure 6. Spatial distribution of the decadal change in the TG90p index, calculated from the summer seasonal TG90p from 1976 to 2005 as a linear trend for each land grid element, for TSMP and the CORDEX ensemble.

The TSMP-simulated TG90p index is consistent with that of MPI-ESM-LR driven RCMs from the CORDEX ensemble, although there are some regional differences (see Fig. 4a-d, Fig. 5a-d, Fig. 6a-d). On average over the focus domain, TSMP yields the lowest mean, variability, and decadal change of the TG90p index, among the MPI-ESM-LR driven RCMs (see Tables A1, A2, A3 in Appendix A). A comparison of TSMP simulations and MPI-ESM-LR driven RCMs from the CORDEX ensemble shows that the largest differences in the TG90p mean and variability occur in the Iberian Peninsula, with TSMP giving the lowest values. In this region, the mean TG90p index is equal to 10.36 days in TSMP and 12.54-12.75 days in the CORDEX RCMs driven by MPI-ESM-LR, at the same time the TG90p variability reaches 6.17 days in TSMP and 8.01-9.59 days in the CORDEX RCMs driven by MPI-ESM-LR (see Tables A1, A2 in Appendix A). As for the decadal change of the TG90p index, TSMP as well as MPI-ESM-LR driven RCMs from the CORDEX ensemble simulate a negative trend in Scandinavia and a positive trend in Southern and Central Europe. The largest differences in the decadal change of the TG90p index appear again in the Iberian Peninsula, with an increase of 2.26 days per decade in TSMP and 3.66-4.25 days per decade in the MPI-ESM-LR driven RCMs from the CORDEX ensemble (see A3 in Appendix A). Different responses to groundwater coupling in different PRUDENCE regions can be explained by the soil moisture-temperature feedback associated with different evaporative regimes, energy-limited in Scandinavia and Northern Europe versus moisture-limited in Southern Europe (e.g., Koster et al., 2009; Seneviratne et al., 2010; Jach et al., 2022).

3.2 Heat events of different durations

The number of heat events (i.e., series of consecutive hot days) of different durations that occur on average over the focus domain in the summer seasons between 1976 and 2005 is presented in Fig. 7a. The total number of heat events (of any duration) per summer per land grid element of the focus domain ranges from the lowest value of 4.18 in COSMO-crCLIM driven by CNRM-CM5 to the highest of 4.86 in REMO2015 driven by NCC-NorESM1-M. The ratio of the number of heat events between RCMs from the CORDEX ensemble and TSMP (blue lines in Fig. 7a) increases towards heat events of long durations ($\geq$6 days), i.e., heat waves. It indicates that TSMP systematically simulates the least number of heat waves compared to the CORDEX ensemble. A comparison of RCMs within the CORDEX ensemble suggests that REMO tends to simulate more heat waves of long durations than COSMO.

Different RCMs simulate different spatial distributions of heat waves for the period 1976-2005, shown in Fig. 8, whereas TSMP generates the smoothest distribution compared to the CORDEX ensemble, resulting in the smallest regional differences (see indicated standard deviations in Fig. 8). Averaged over the focus domain, the decadal number of heat waves in the considered RCMs lies between the lowest value in TSMP (3.25) and the highest in REMO2015 driven by IPSL-CM5A-LR (5.09), see Table B1 in Appendix B. Comparing TSMP and MPI-ESM-LR driven RCMs from the CORDEX ensemble, TSMP simulates the most heat waves towards Central Europe, while the CORDEX RCMs simulate the highest number of heat waves towards Southern Europe; strong differences are observed on the Iberian Peninsula and in the Mediterranean, and the smallest differences are in Scandinavia (see Fig. 8a-d and Table B1 in Appendix B). When comparing TSMP with the most compatible RCM from the CORDEX ensemble, i.e., CCLM4-8-17 forced by MPI-ESM-LR, TSMP simulates fewer heat waves in all PRUDENCE regions except Mid-Europe.

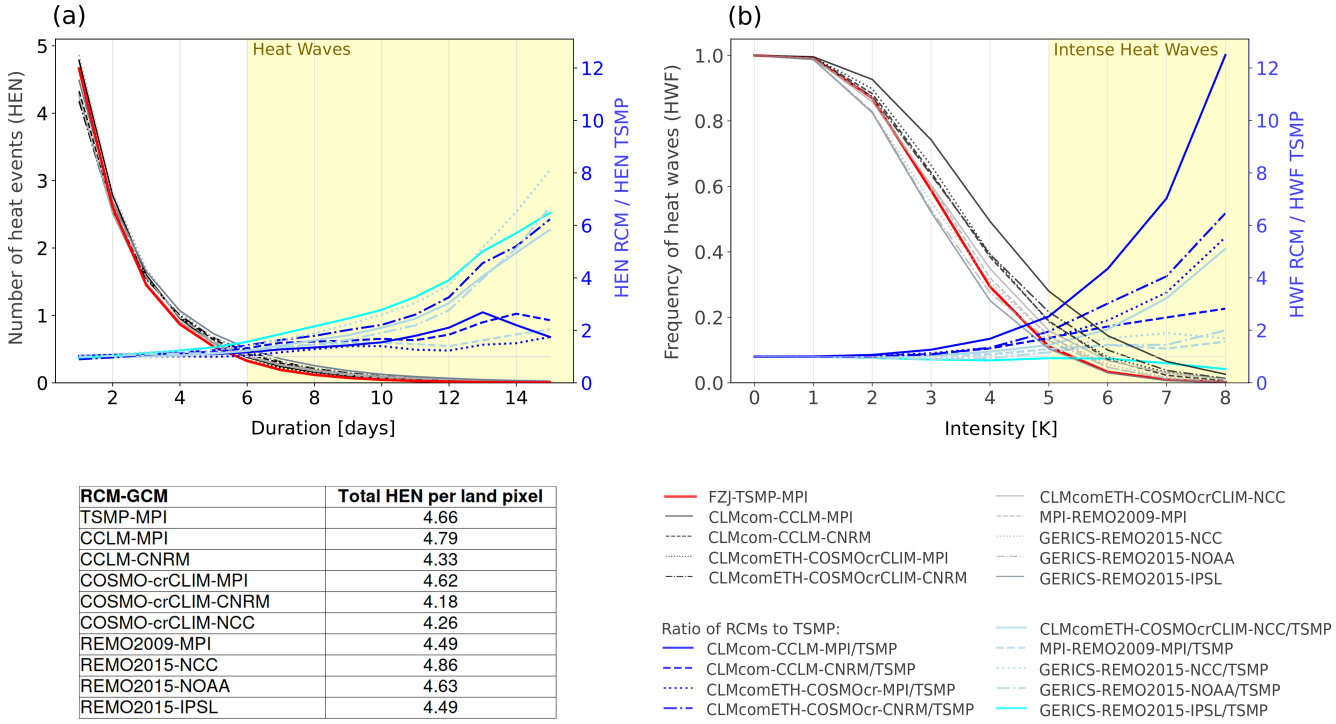

RCM-GCM	Total HEN per land pixel
TSMP-MPI	4.66
CCLM-MPI	4.79
CCLM-CNRM	4.33
COSMO-crCLIM-MPI	4.62
COSMO-crCLIM-CNRM	4.18
COSMO-crCLIM-NCC	4.26
REMO2009-MPI	4.49
REMO2015-NCC	4.86
REMO2015-NOAA	4.63
REMO2015-IPSL	4.49

Figure 7. (a) Average number of summer heat events (HEN, y-axis) of duration equal to or greater than a given number of days (x-axis) as a function of this number of days; the averaging is performed over the total number of land grid elements of the focus domain and 30 years, from 1976 to 2005. (b) Frequency of heat waves (HWF, y-axis) with intensities equal to or higher than a value indicated on the abscissa, that occur in the focus domain from 1976 to 2005 as a function of this intensity. The panels also show the ratio of HEN and HWN values between RCMs from the CORDEX ensemble and TSMP. Data are taken from the summer seasons between 1976 and 2005 with respect to the reference period 1961-1990 in each RCM. The representation of the dependencies is adopted from the work of Vautard et al. (2013a).

The contribution of heat waves to the total number of hot days during the summer seasons of 1976-2005 is presented in Fig. 9, with TSMP giving the lowest value (22.38 %) on average in the focus domain (Table B2 in Appendix B). The highest value is registered in REMO2015 driven by IPSL-CM5A-LR, where heat waves account for 34.40 %. Therefore, the proportion of heat events that do not belong to heat waves, i.e., with a duration of less than 6 days, is higher in TSMP compared to the CORDEX ensemble. On average, in the considered RCMs, Scandinavia is the region with the largest contribution of heat waves to the total number of hot days, which is expected to coincide with the region of the highest number of heat waves. Eastern Europe is the region with the least number of heat waves and the lowest contribution of heat waves to the total number of hot days. The largest discrepancy between TSMP and the MPI-ESM-LR driven RCMs from the CORDEX ensemble appear in the Iberian Peninsula and the Mediterranean.

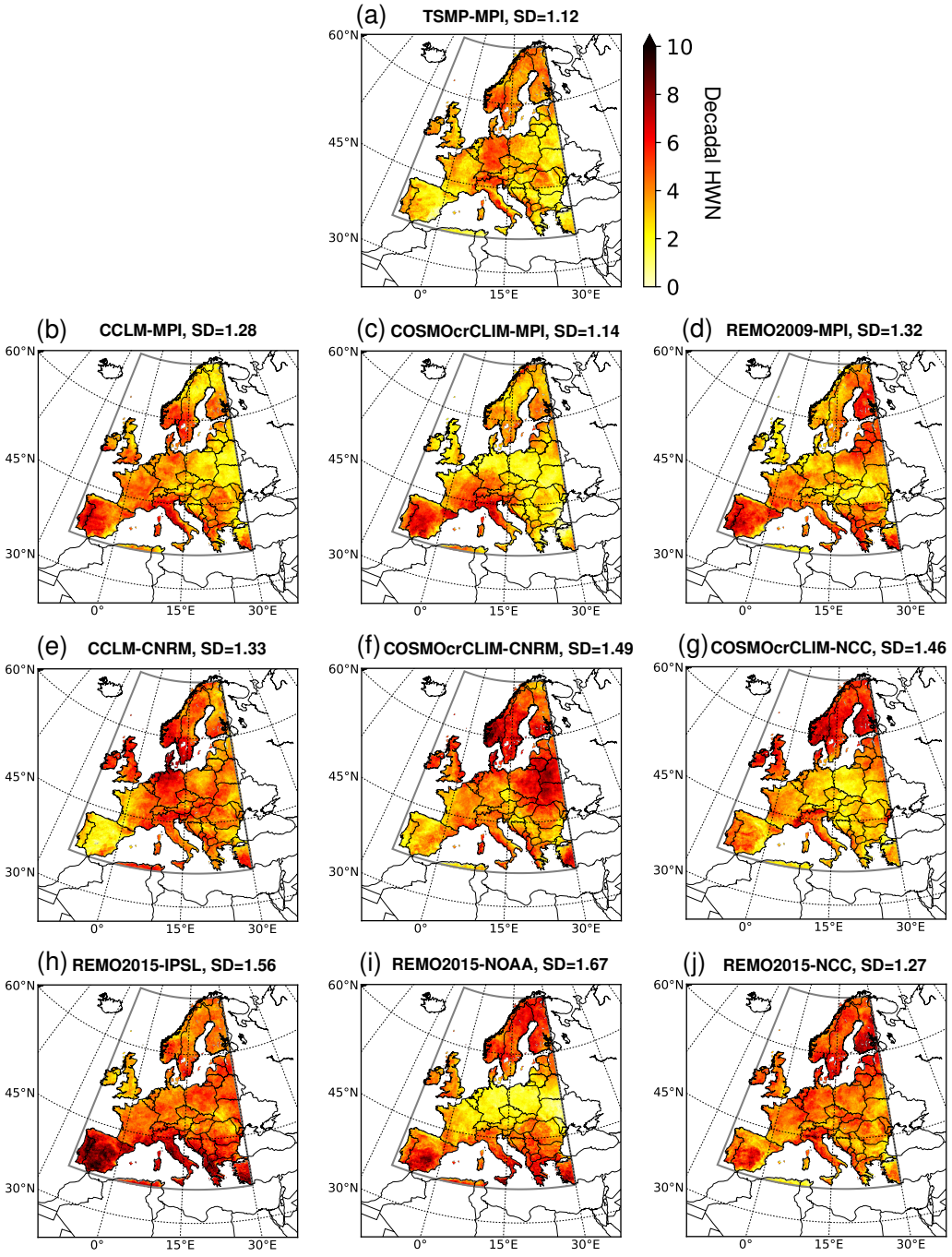

Figure 8. Spatial distribution of the decadal number of heat waves (HWN) based on data from 1976 to 2005 with respect to the reference period 1961-1990, in TSMP and the CORDEX ensemble. The standard deviation (SD) is indicated in every figure.

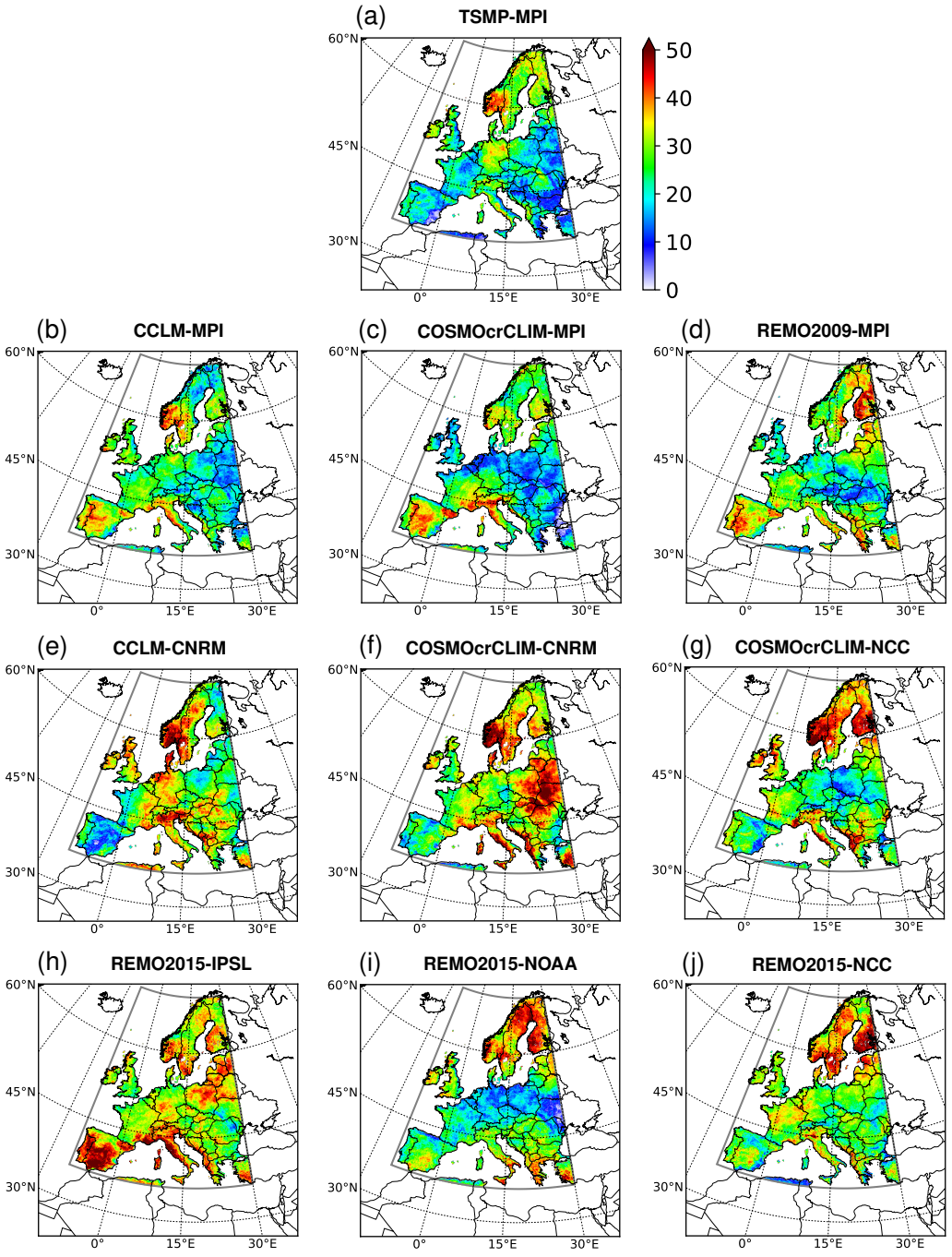

Figure 9. Contribution of heat waves to the number of hot days [%], calculated from the total number of heat waves and hot days accumulated between 1976 and 2005, for TSMP and the CORDEX ensemble.

3.3 Heat waves of different intensities

The dependence of the frequency of heat waves that occurred between 1976 and 2005 in the focus domain on their intensities is shown in Fig. 7b. The maximum frequency of heat waves is equal to 1 for an intensity greater than 0, since all heat waves are taken into account for each RCM. The ratio of the frequency of heat waves between RCMs from the CORDEX ensemble and TSMP (blue lines in Fig. 7b) increases toward intense heat waves ($\geq$5 K). It shows a systematic behavior of TSMP to simulate less intense heat waves on average in the focus domain compared to the CORDEX ensemble. The largest discrepancy is found between TSMP and CCLM4-8-17 forced by MPI-ESM-LR (blue solid line in Fig. 7b), up to a factor of 12 or even more, depending on the intensity considered. Overall, when comparing RCMs within the CORDEX ensemble, COSMO tend to simulate more intense heat waves than REMO. And REMO2015 driven by IPSL-CM5A-LR simulates even less intense heat waves than TSMP.

The spatial distribution of the intense heat waves is presented in Fig. 10, with their highest frequency in France and lowest in the Alps, on average among the considered RCMs (Table B3 in Appendix B). Note that the frequency here is calculated relative to the total number of heat waves in each RCM, see Sec. 2.4 for definitions. The mean frequency of intense heat waves in the focus domain ranges from the lowest value in REMO2015 driven by IPSL-CM5A-LR (0.174) to the highest value in CCLM4-8-17 driven by MPI-ESM-LR (0.301). It indicates that 17.4-30.1 % of all simulated heat waves exceed the intensity of 5 K. When comparing TSMP with the most compatible RCM from the CORDEX ensemble, i.e., CCLM4-8-17 forced by MPI-ESM-LR, TSMP simulates a lower frequency of intense heat waves in all PRUDENCE regions except Scandinavia. The largest discrepancies between TSMP and CCLM4-8-17 forced by MPI-ESM-LR are observed in France, where TSMP simulates 24.6 % and CCLM4-8-17 46.8 % of all heat waves as intense, the smallest differences are found in Scandinavia, with 19.3 % intense heat waves in TSMP and 17.5 % in CCLM4-8-17. It is important to note that the regions of the highest number of heat waves do not necessarily coincide with the regions of the highest number of intense heat waves (see Fig. 8 and Fig. 10), in other words, intense heat waves do not necessarily occur where the majority of heat waves are detected. The origin of these differences should be further investigated and is beyond the scope of this analysis.

4 Summary and conclusions

We presented a first-of-its-kind TSMP dataset forced by the CMIP5 MPI-ESM-LR GCM boundary conditions, with an explicit representation of 3D groundwater hydrodynamics, in the context of dynamical downscaling of GCMs for climate change studies. By comparing the TSMP simulation results with those of the RCMs with simplified groundwater dynamics from the CORDEX ensemble, we investigated the impact of groundwater dynamics on the statistics of simulated heat events in historical regional climate simulations over Europe, with potential implications for climate change projections. In particular, we examined the characteristics of heat events of different durations and intensities during the summer season between 1976 and 2005 with respect to the reference period 1961-1990 in each RCM.

Our results show that the characteristics of the TSMP-simulated heat events are consistent with the CORDEX ensemble, although there are systematic differences that we attribute to groundwater coupling. TSMP simulates lower mean values as

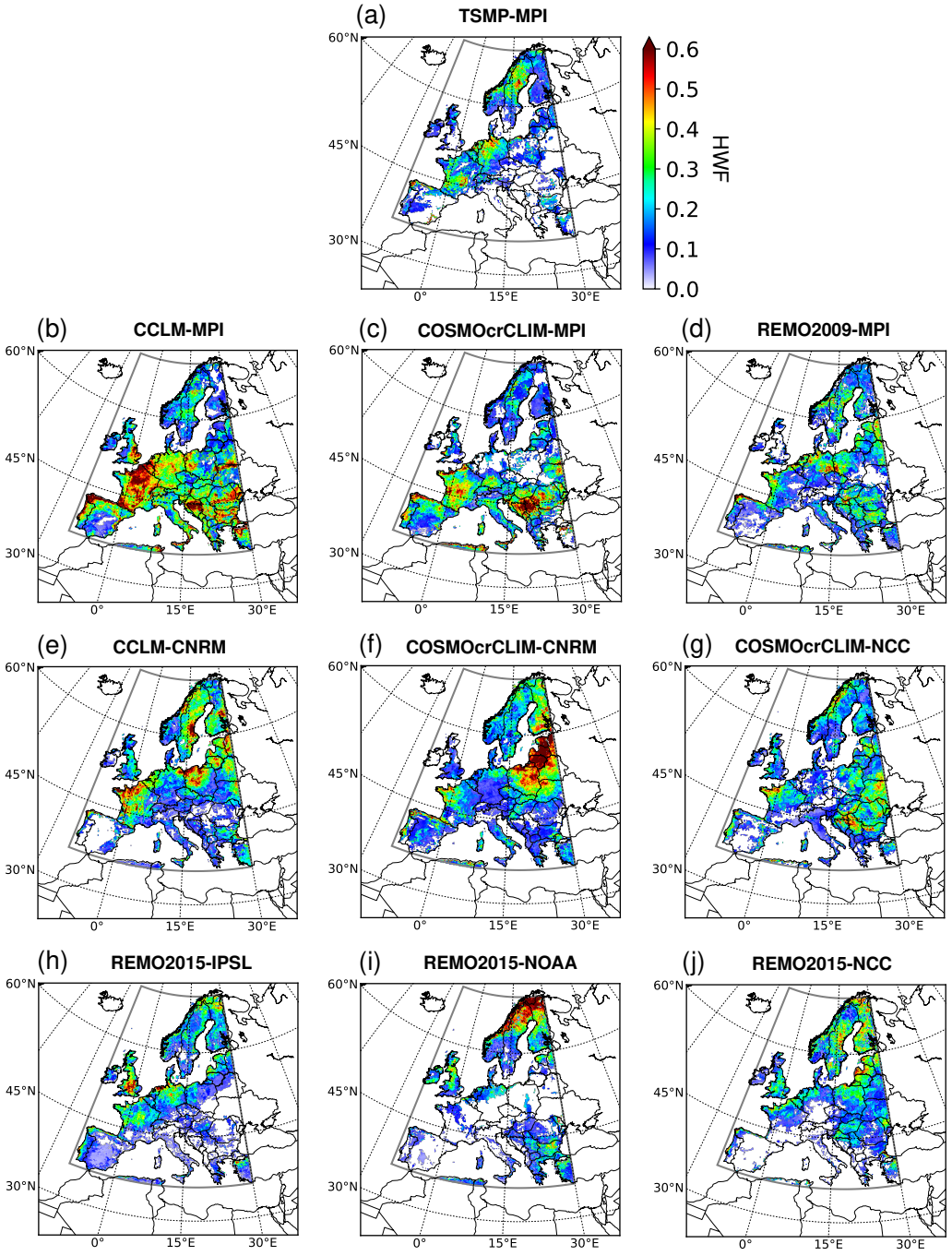

Figure 10. Frequency of heat waves (HWF) with intensities above 5 K occurring between 1976 and 2005 with respect to the reference period 1961-1990, in TSMP and the CORDEX ensemble.

well as lower interannual variability in the number of hot days on average in Europe, compared to the CORDEX ensemble. The decadal change in the number of hot days is also lower in TSMP compared to the CORDEX ensemble mean. TSMP simulates fewer heat waves and tends to simulate less intense heat waves compared to the CORDEX ensemble. The most sensitive regions to groundwater coupling are the Iberian Peninsula and the Mediterranean, while Scandinavia is the least sensitive.

Comparing TSMP with the most compatible RCM from the CORDEX ensemble, i.e., CCLM4-8-17 forced by MPI-ESM-LR, we find that TSMP simulates lower values of hot days and heat waves characteristics, on average over the focus domain, based on the 1976-2005 data, namely:

- mean number of hot days: 10.95 days in TSMP and 11.80 days in CCLM4-8-17;
- variability of the number of hot days: 6.80 days TSMP and 8.33 days in CCLM4-8-17;
- decadal change in the number of hot days: 1.53 days in TSMP and 1.86 days in CCLM4-8-17;
- decadal number of heat waves: 3.25 in TSMP and 3.78 in CCLM4-8-17;
- contribution of heat waves to the number of hot days: 22.38 % in TSMP and 24.96 % in CCLM4-8-17;
- frequency of intense heat waves: 0.193 in TSMP and 0.301 in CCLM4-8-17.

This study clearly indicates that a coupled regional climate system with a closed terrestrial water cycle, such as TSMP, systematically simulates a different climatology of heat events compared to uncoupled RCMs. The explicit representation of groundwater hydrodynamics in RCMs may be a key for the reduction of biases in the simulated duration and intensity of heat waves, particularly in Southern Europe.

Appendix A: Average characteristics of hot days for different regions

RCMs \ Regions	BI	IP	FR	ME	SC	AL	MD	EA	FD
TSMP-MPI	10.95	10.36	11.50	11.76	10.00	12.20	11.40	11.13	10.95
CCLM-MPI	11.49	12.64	12.46	12.80	10.42	13.27	12.62	11.50	11.80
COSMO-crCLIM-MPI	9.94	12.54	11.28	11.18	9.93	12.91	12.03	10.82	11.10
REMO2009-MPI	9.45	12.75	10.82	10.90	10.24	11.56	11.59	11.28	11.14
CCLM4-CNRM	12.89	9.66	10.93	12.62	12.06	10.74	10.49	11.16	11.32
COSMO-crCLIM-CNRM	12.05	10.14	9.87	10.87	13.87	10.15	9.85	11.26	11.46
COSMO-crCLIM-NCC	12.78	11.66	11.21	10.96	12.84	10.76	9.02	9.91	11.10
REMO2015-NCC	12.61	12.89	12.06	12.86	13.31	13.27	11.27	12.95	12.72
REMO2015-IPSL	9.56	15.00	11.45	11.48	11.29	12.64	15.25	11.63	12.38
REMO2015-NOAA	9.96	15.33	10.54	8.98	12.21	11.56	13.87	10.05	11.77

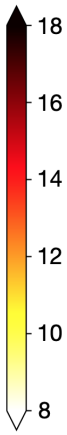

Table A1. Mean number of hot days, i.e. TG90p index [days], for the summer season averaged between 1976 and 2005 with respect to the reference period 1961-1990, in TSMP and the CORDEX ensemble, for the focus domain (FD) and the PRUDENCE regions: British Isles (BI), Iberian Peninsula (IP), France (FR), Mid-Europe (ME), Scandinavia (SC), Alps (AL), Mediterranean (MD), Eastern Europe (EA); see Fig. 4 for the spatial distribution.

RCMs \ Regions	BI	IP	FR	ME	SC	AL	MD	EA	FD
TSMP-MPI	7.68	6.17	6.92	7.43	6.26	7.50	6.93	6.93	6.80
CCLM-MPI	8.50	9.59	8.30	8.53	7.45	8.82	9.34	8.02	8.33
COSMO-crCLIM-MPI	6.75	8.01	6.56	6.90	6.56	8.56	9.00	7.42	7.38
REMO2009-MPI	6.73	8.94	7.36	6.81	6.48	7.39	9.37	7.62	7.62
CCLM4-CNRM	8.07	6.37	8.72	10.00	8.47	7.32	8.28	8.17	8.21
COSMO-crCLIM-CNRM	8.50	6.84	7.38	7.42	10.22	8.38	8.19	10.31	8.90
COSMO-crCLIM-NCC	9.24	6.89	7.91	7.41	10.06	8.73	8.79	7.59	8.37
REMO2015-NCC	9.94	8.05	7.21	8.57	12.21	8.48	8.86	8.77	9.42
REMO2015-IPSL	7.74	9.51	8.16	8.39	8.94	9.60	10.13	8.40	8.97
REMO2015-NOAA	6.88	8.71	6.18	5.87	10.24	8.05	10.49	8.11	8.69

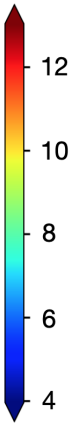

Table A2. Variability of the hot days number, i.e. TG90p index [days], calculated from the summer seasonal TG90p during 1976-2005 as the standard deviation at each land grid element, for TSMP and the CORDEX ensemble, for the focus domain (FD) and the PRUDENCE regions: British Isles (BI), Iberian Peninsula (IP), France (FR), Mid-Europe (ME), Scandinavia (SC), Alps (AL), Mediterranean (MD), Eastern Europe (EA); see Fig. 5 for the spatial distribution.

RCMs \ Regions	BI	IP	FR	ME	SC	AL	MD	EA	FD
TSMP-MPI	0.62	2.26	2.90	1.52	-0.98	3.33	3.74	1.84	1.53
CCLM-MPI	1.39	4.25	3.49	2.03	-0.89	3.29	4.40	1.21	1.86
COSMO-crCLIM-MPI	0.79	3.66	2.87	1.98	-0.62	4.02	2.86	1.47	1.68
REMO2009-MPI	1.80	3.69	3.29	2.67	0.15	2.50	2.65	1.29	1.88
CCLM4-CNRM	3.56	2.78	3.52	3.40	3.29	2.88	1.66	0.43	2.35
COSMO-crCLIM-CNRM	3.00	1.76	1.34	1.36	2.95	1.49	2.54	0.08	1.77
COSMO-crCLIM-NCC	4.50	1.58	3.56	2.43	4.09	1.32	-1.24	0.52	1.87
REMO2015-NCC	3.92	2.64	2.23	2.51	3.08	3.17	1.97	2.85	2.71
REMO2015-IPSL	0.55	3.89	0.57	0.23	0.87	1.27	2.22	-0.20	1.13
REMO2015-NOAA	1.11	5.18	1.44	0.13	4.27	1.27	3.49	1.16	2.68

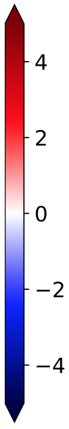

Table A3. Decadal change in the number of hot days, i.e. TG90p index [days], calculated from the summer seasonal TG90p from 1976 to 2005 as a linear trend for each land grid element, for TSMP and the CORDEX ensemble, for the focus domain (FD) and the PRUDENCE regions: British Isles (BI), Iberian Peninsula (IP), France (FR), Mid-Europe (ME), Scandinavia (SC), Alps (AL), Mediterranean (MD), Eastern Europe (EA); see Fig. 6 for the spatial distribution.

Appendix B: Average characteristics of heat waves for different regions

RCMs \ Regions	BI	IP	FR	ME	SC	AL	MD	EA	FD
TSMP-MPI	3.33	2.51	3.15	4.01	3.83	4.13	3.04	2.74	3.25
CCLM-MPI	3.85	4.88	4.20	3.84	3.59	4.50	4.48	2.86	3.78
COSMO-crCLIM-MPI	2.54	4.99	3.73	2.78	3.46	5.27	3.59	2.34	3.35
REMO2009-MPI	2.70	5.25	4.17	3.30	4.17	3.50	4.40	3.24	3.89
CCLM4-CNRM	5.25	2.53	3.57	5.31	4.69	5.09	4.43	4.15	4.31
COSMO-crCLIM-CNRM	4.84	3.18	3.69	4.09	5.65	4.03	4.18	5.27	4.63
COSMO-crCLIM-NCC	5.24	3.66	3.86	3.15	5.61	4.10	3.43	2.92	3.97
REMO2015-NCC	4.42	4.23	4.15	4.64	5.52	4.69	3.92	4.01	4.49
REMO2015-IPSL	3.21	7.25	4.49	4.23	4.44	5.59	6.77	4.58	5.09
REMO2015-NOAA	3.91	4.93	3.10	2.02	5.03	3.57	5.42	2.62	3.95

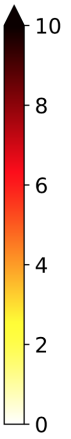

Table B1. Decadal number of heat waves based on data from 1976 to 2005 with respect to the reference period 1961-1990, in TSMP and the CORDEX ensemble, for the focus domain (FD) and the PRUDENCE regions: British Isles (BI), Iberian Peninsula (IP), France (FR), Mid-Europe (ME), Scandinavia (SC), Alps (AL), Mediterranean (MD), Eastern Europe (EA); see Fig. 8 for the spatial distribution.

RCMs \ Regions	BI	IP	FR	ME	SC	AL	MD	EA	FD
TSMP-MPI	25.36	17.47	19.62	25.61	29.87	24.40	19.33	17.79	22.38
CCLM-MPI	27.90	31.19	26.29	24.34	26.50	27.79	26.67	18.82	24.96
COSMO-crCLIM-MPI	18.78	31.96	25.50	18.49	27.59	33.62	24.46	16.27	23.46
REMO2009-MPI	21.81	33.04	28.35	22.39	32.63	23.50	30.18	21.92	27.22
CCLM4-CNRM	34.53	18.35	25.45	33.01	31.69	37.74	34.53	28.08	29.72
COSMO-crCLIM-CNRM	29.75	23.36	29.21	29.31	36.52	32.75	35.54	38.21	33.11
COSMO-crCLIM-NCC	34.70	23.94	30.71	23.12	39.04	30.05	33.07	23.70	29.61
REMO2015-NCC	30.16	25.39	32.05	29.06	38.37	29.72	27.54	26.69	30.20
REMO2015-IPSL	30.39	41.20	30.57	31.56	35.26	38.26	36.73	31.75	34.40
REMO2015-NOAA	30.77	25.20	21.41	16.51	37.52	24.58	32.54	19.36	26.97

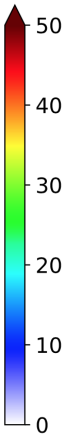

Table B2. Contribution of heat waves to the number of hot days [%], calculated from the total number of heat waves and hot days accumulated between 1976 and 2005, for TSMP and the CORDEX ensemble, for the focus domain (FD) and the PRUDENCE regions: British Isles (BI), Iberian Peninsula (IP), France (FR), Mid-Europe (ME), Scandinavia (SC), Alps (AL), Mediterranean (MD), Eastern Europe (EA); see Fig. 9 for the spatial distribution.

RCMs \ Regions	BI	IP	FR	ME	SC	AL	MD	EA	FD
TSMP-MPI	0.118	0.189	0.246	0.233	0.193	0.145	0.171	0.148	0.193
CCLM-MPI	0.246	0.305	0.468	0.395	0.175	0.326	0.318	0.319	0.301
COSMO-crCLIM-MPI	0.181	0.246	0.361	0.216	0.152	0.213	0.262	0.318	0.241
REMO2009-MPI	0.173	0.156	0.207	0.230	0.211	0.125	0.180	0.218	0.202
CCLM4-CNRM	0.185	0.199	0.356	0.244	0.290	0.121	0.125	0.218	0.233
COSMO-crCLIM-CNRM	0.111	0.187	0.236	0.157	0.309	0.106	0.143	0.293	0.232
COSMO-crCLIM-NCC	0.160	0.188	0.234	0.163	0.193	0.105	0.165	0.268	0.204
REMO2015-NCC	0.181	0.173	0.163	0.166	0.267	0.082	0.123	0.184	0.205
REMO2015-IPSL	0.287	0.112	0.219	0.214	0.203	0.112	0.084	0.108	0.174
REMO2015-NOAA	0.213	0.094	0.120	0.197	0.294	0.101	0.144	0.141	0.213

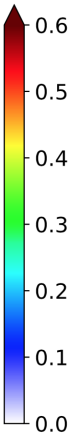

Table B3. Frequency of heat waves with intensities greater than 5 K based on data from 1976 to 2005 with respect to the reference period 1961-1990, in TSMP and the CORDEX ensemble, for the focus domain (FD) and the PRUDENCE regions: British Isles (BI), Iberian Peninsula (IP), France (FR), Mid-Europe (ME), Scandinavia (SC), Alps (AL), Mediterranean (MD), Eastern Europe (EA); see Fig. 10 for the spatial distribution.

Code and data availability. The TSMP v1.2.2 used in this work is available through https://github.com/HPSCTerrSys/TSMP GIT repository. The TSMP dataset forced by MPI-ESM-LR r1i1p1 can be accessed at https://datapub.fz-juelich.de/slts/regional_climate_tsmp_hi-cam/ as open access research data.

Author contributions. The study was designed by S.K. with contributions by K.G., L.P-S., and N.W.. L.P.-S. performed the model simulations and data processing, N.W. provided technical and programming support, C.H. provided setups, configuration, and workflow support. The analysis was developed and conducted by L.P.-S. with further inputs from S.K. and K.G.. L.P.-S. wrote the manuscript. All co-authors contributed to the interpretation of the results, active discussions, and revisions of the paper. The work was done under the supervision of S.K..

Competing interests. The authors declare that they have no conflict of interest.

Acknowledgements. This work was funded by the Helmholtz Association of German Research Centres (HGF) under the HI-CAM project (Helmholtz Initiative Climate Adaptation and Mitigation) and by the German Ministry of Education and Research (Bundesministerium für Bildung und Forschung, BMBF) under the ClimXtreme project. We are grateful to the Max-Planck Institute for performing MPI-ESM-LR r1i1p1 GCM experiment and the German Climate Computing Centre (DKRZ) for providing the MPI-ESM-LR dataset. We thank the EURO-CORDEX climate modelling groups for producing and making available their model output. The authors gratefully acknowledge the Earth System Modelling Project (ESM) for funding this work by providing computing time on the ESM partition of the supercomputer JUWELS at the Jülich Supercomputing Centre (JSC) under the ESM project ID JIBG35. In addition, we thank the Centre for High-Performance Scientific Computing in Terrestrial Systems (Geoverbund ABC/J, http://www.hpsc-terrsys.de) and the JSC for the computational support. Finally, we thank three anonymous reviewers for the constructive comments that helped improve the paper.

References

Alexander, L. V., Zhang, X., Peterson, T. C., Caesar, J., Gleason, B., Klein Tank, A. M. G., Haylock, M., Collins, D., Trewin, B., Rahimzadeh, F., Tagipour, A., Rupa Kumar, K., Revadekar, J., Griffiths, G., Vincent, L., Stephenson, D. B., Burn, J., Aguilar, E., Brunet, M., Taylor, M., New, M., Zhai, P., Rusticucci, M., and Vazquez-Aguirre, J. L.: Global observed changes in daily climate extremes of temperature and precipitation, J. Geophys. Res. Atmos., 111, D05109, https://doi.org/10.1029/2005JD006290, 2006.

Amengual, A., Homar, V., Romero, R., Brooks, H., Ramis, C., Gordaliza, M., and Alonso, S.: Projections of heat waves with high impact on human health in Europe, Glob. Planet. Change, 119, 71–84, https://doi.org/10.1016/j.gloplacha.2014.05.006, 2014.

Baldauf, M., Seifert, A., Förstner, J., Majewski, D., Raschendorfer, M., and Reinhardt, T.: Operational Convective-Scale Numerical Weather Prediction with the COSMO Model: Description and Sensitivities, Mon. Weather Rev., 139, 3887–3905, https://doi.org/10.1175/MWR-D-10-05013.1, 2011.

Barlage, M., Tewari, M., Chen, F., Miguez-Macho, G., Yang, Z.-L., and Niu, G.-Y.: The effect of groundwater interaction in North American regional climate simulations with WRF/Noah-MP, Clim. Change, 129, 485–498, https://doi.org/10.1007/s10584-014-1308-8, 2015.

Barlage, M., Chen, F., Rasmussen, R., Zhang, Z., and Miguez-Macho, G.: The Importance of Scale-Dependent Groundwater Processes in Land-Atmosphere Interactions Over the Central United States, Geophysical Research Letters, 48, e2020GL092 171, https://doi.org/10.1029/2020GL092171, 2021.

Barriopedro, D., Fischer, E. M., Luterbacher, J., Trigo, R. M., and R., G.-H.: The Hot Summer of 2010: Redrawing the Temperature Record Map of Europe, Science, 332, 220–224, https://doi.org/10.1126/science.1201224, 2011.

Bellprat, O., Kotlarski, S., Lüthi, D., Elía, R. D., Frigon, A., Laprise, R., and Schär, C.: Objective Calibration of Regional Climate Models: Application over Europe and North America, Journal of Climate, 29, 819–838, https://doi.org/10.1175/JCLI-D-15-0302.1, 2016.

Bentsen, M., Bethke, I., Debernard, J. B., Iversen, T., Kirkevåg, A., Seland, Ø., Drange, H., Roelandt, C., Seierstad, I. A., Hoose, C., and Kristjánsson, J. E.: The Norwegian Earth System Model, NorESM1-M – Part 1: Description and basic evaluation of the physical climate, Geosci. Model Dev., 6, 687–720, https://doi.org/10.5194/gmd-6-687-2013, 2013.

Bosello, F., Roson, R., and Tol, R.: Economy-wide Estimates of the Implications of Climate Change: Sea Level Rise, Environ. Resource Econ., 37, 549–571, https://doi.org/10.1007/s10640-006-9048-5, 2007.

Campoy, A., Ducharne, A., Cheruy, F., Hourdin, F., Polcher, J., and Dupont, J. C.: Response of land surface fluxes and precipitation to different soil bottom hydrological conditions in a general circulation model, J. Geophys. Res. Atmos., 118, 10 725–10 739, https://doi.org/10.1002/jgrd.50627, 2013.

Christensen, J. H. and Christensen, O. B.: A summary of the PRUDENCE model projections of changes in European climate by the end of this century, Clim. Change, 81, 7–30, https://doi.org/10.1007/s10584-006-9210-7, 2007.

Christidis, N., Jones, G., and Stott, P.: Dramatically increasing chance of extremely hot summers since the 2003 European heatwave, Nature Clim. Change, 5, 46–50, https://doi.org/10.1038/nclimate2468, 2015.

Ciscar, J.-C., Iglesias, A., Feyen, L., Szabó, L., Van Regemorter, D., Amelung, B., Nicholls, R., Watkiss, P., Christensen, O. B., Dankers, R., Garrote, L., Goodess, C. M., Hunt, A., Moreno, A., Richards, J., and Soria, A.: Physical and economic consequences of climate change in Europe, Proc. Natl. Acad. Sci., 108, 2678–2683, https://doi.org/10.1073/pnas.1011612108, 2011.

Cornes, R. C., van der Schrier, G., van den Besselaar, E. J. M., and Jones, P. D.: An Ensemble Version of the E-OBS Temperature and Precipitation Data Sets, J. Geophys. Res. Atmos., 123, 9391–9409, https://doi.org/10.1029/2017JD028200, 2018.

Dee, D. P., Uppala, S. M., Simmons, A. J., Berrisford, P., Poli, P., Kobayashi, S., Andrae, U., Balmaseda, M. A., Balsamo, G., Bauer, P., Bechtold, P., Beljaars, A. C. M., van de Berg, L., Bidlot, J., Bormann, N., Delsol, C., Dragani, R., Fuentes, M., Geer, A. J., Haimberger, L., Healy, S. B., Hersbach, H., Hólm, E. V., Isaksen, L., Kallberg, P., Koehler, M., Matricardi, M., McNally, A. P., Monge-Sanz, B. M., Morcrette, J.-J., Park, B.-K., Peubey, C., de Rosnay, P., Tavolato, C., Thépaut, J.-N., and Vitart, F.: The ERA-Interim reanalysis: configuration and performance of the data assimilation system, Q. J. R. Meteorol. Soc., 137, 553–597, https://doi.org/10.1002/qj.828, 2011.

Déqué, M., Rowell, D. P., Lüthi, D., Giorgi, F., Christensen, J. H., Rockel, B., Jacob, D., Kjellström, E., de Castro, M., and van den Hurk, B.: An intercomparison of regional climate simulations for Europe: assessing uncertainties in model projections, Clim. Change, 81, 53–70, https://doi.org/10.1007/s10584-006-9228-x, 2007.

Déqué, M., Somot, S., Sanchez-Gomez, E., Goodess, C. M., Jacob, D., Lenderink, G., and Christensen, O. B.: The spread amongst ENSEMBLES regional scenarios: regional climate models, driving general circulation models and interannual variability, Clim. Change, 38, 951–964, https://doi.org/10.1007/s00382-011-1053-x, 2012.

Dirmeyer, P. A., Balsamo, G., Blyth, E. M., Morrison, R., and Cooper, H. M.: Land-Atmosphere Interactions Exacerbated the Drought and Heatwave Over Northern Europe During Summer 2018, AGU Advances, 2, e2020AV000283, https://doi.org/10.1029/2020AV000283, 2021.

Doms, G., Föorstner, J., Heise, E., Herzog, H.-J., Mironov, D., Raschendorfer, M., Reinhardt, T., Ritter, B., Schrodin, R., Schulz, J.-P., and Vogel, G.: Consortium for small-scale modelling: A description of the nonhydrostatic regional COSMO model. Part II: Physical parameterization, Tech. rep., https://doi.org/10.5676/DWD_pub/nwv/cosmo-doc_5.00_II, 2013.

Dufresne, J.-L., Foujols, M.-A., Denvil, S., and et al.: Climate change projections using the IPSL-CM5 Earth System Model: from CMIP3 to CMIP5, Clim. Dyn., 40, 2123–2165, https://doi.org/10.1007/s00382-012-1636-1, 2013.

Dunne, J. P., John, J. G., Adcroft, A. J., Griffies, S. M., Hallberg, R. W., Shevliakova, E., Stouffer, R. J., Cooke, W., Dunne, K. A., Harrison, M. J., Krasting, J. P., Malyshev, S. L., Milly, P. C. D., Phillipps, P. J., Sentman, L. T., Samuels, B. L., Spelman, M. J., Winton, M., Wittenberg, A. T., and Zadeh, N.: GFDL's ESM2 Global Coupled Climate–Carbon Earth System Models. Part I: Physical Formulation and Baseline Simulation Characteristics, J. Clim., 25, 6646–6665, https://doi.org/10.1175/JCLI-D-11-00560.1, 2012.

Duscher, K., Günther, A., Richts, A., Clos, P., Philipp, U., and Struckmeier, W.: The GIS layers of the "International Hydrogeological Map of Europe 1:1,500,000" in a vector format, Hydrogeol. J., 23, 1867–1875, https://doi.org/10.1007/s10040-015-1296-4, 2015.

Eltahir, E. A. B.: A Soil Moisture-Rainfall Feedback Mechanism: 1. Theory and observations, Water Resour. Res., 34, 765–776, https://doi.org/10.1029/97WR03499, 1998.

Erdenebat, E. and Tomonori, S.: Role of soil moisture-atmosphere feedback during high temperature events in 2002 over Northeast Eurasia, Prog. Earth. Planet. Sci., 5, 37, https://doi.org/10.1186/s40645-018-0195-4, 2018.

Evin, G., Somot, S., and Hingray, B.: Balanced estimate and uncertainty assessment of European climate change using the large EURO-CORDEX regional climate model ensemble, Earth Syst. Dyn., 12, 1543–1569, https://doi.org/10.5194/esd-12-1543-2021, 2021.

FAO: FAO/UNESCO Soil Map of the World, Revised Legend, with corrections and updates, World Soil Resources Report 60, FAO, Rome, https://www.fao.org/3/bl892e/bl892e.pdf, 1988.

Fernandez-Granja, J. A., Casanueva, A., Bedia, J., and Fernandez, J.: Improved atmospheric circulation over Europe by the new generation of CMIP6 earth system models, Clim. Dyn., 56, 3527–3540, https://doi.org/10.1007/s00382-021-05652-9, 2021.

Fernández, J., Frías, M. D., Cabos, W. D., Cofiño, A. S., Domínguez, M., Fita, L., Gaertner, M. A., García-Díez, M., Gutiérrez, J. M., Jiménez-Guerrero, P., Liguori, G., Montávez, J. P., Romera, R., and Sánchez, E.: Consistency of climate change projections from multiple global and regional model intercomparison projects, Clim. Dyn., 52, 1139–1156, https://doi.org/10.1007/s00382-018-4181-8, 2019.

Fischer, E. M. and Schär, C.: Consistent geographical patterns of changes in high-impact European heatwaves, Nat. Geosci., 3, 398–403, https://doi.org/10.1038/ngeo866, 2010.

Fischer, E. M., Seneviratne, S. I., Lüthi, D., and Schär, C.: Contribution of land-atmosphere coupling to recent European summer heat waves, Geophys. Res. Lett., 34, L06707, https://doi.org/10.1029/2006GL029068, 2007.

Frich, P., Alexander, L. V., Della-Marta, P., Gleason, B., Haylock, M., Klein Tank, A. M. G., and Peterson, T.: Observed coherent changes in climatic extremes during the second half of the twentieth century, Clim. Res., 19, 193–212, https://doi.org/10.3354/cr019193, 2002.

Friedl, M., McIver, D., Hodges, J., Zhang, X., Muchoney, D., Strahler, A., Woodcock, C., Gopal, S., Schneider, A., Cooper, A., Baccini, A., Gao, F., and Schaaf, C.: Global land cover mapping from MODIS: algorithms and early results, Remote Sens. Environ., 83, 287–302, https://doi.org/10.1016/S0034-4257(02)00078-0, 2002.

Furusho-Percot, C., Goergen, K., Hartick, C., Kulkarni, K., Keune, J., and Kollet, S.: Pan-European groundwater to atmosphere terrestrial systems climatology from a physically consistent simulation, Sci. Data, 6, 320, https://doi.org/10.1038/s41597-019-0328-7, 2019.

Furusho-Percot, C., Goergen, K., Hartick, C., Poshyvailo-Strube, L., and Kollet, S.: Groundwater Model Impacts Multiannual Simulations of Heat Waves, Geophys. Res. Lett., 49, e2021GL096781, https://doi.org/10.1029/2021GL096781, 2022.

Gasper, F., Goergen, K., Shrestha, P., Sulis, M., Rihani, J., Geimer, M., and Kollet, S.: Implementation and scaling of the fully coupled Terrestrial Systems Modeling Platform (TerrSysMP v1.0) in a massively parallel supercomputing environment – a case study on JUQUEEN (IBM Blue Gene/Q), Geosci. Model Dev., 7, 2531–2543, https://doi.org/10.5194/gmd-7-2531-2014, 2014.

Giorgetta, M. A., Jungclaus, J., Reick, C. H., Legutke, S., Bader, J., Böttinger, M., Brovkin, V., Crueger, T., Esch, M., Fieg, K., Glushak, K., Gayler, V., Haak, H., Hollweg, H.-D., Ilyina, T., Kinne, S., Kornblueh, L., Matei, D., Mauritsen, T., Mikolajewicz, U., Mueller, W., Notz, D., Pithan, F., Raddatz, T., Rast, S., Redler, R., Roeckner, E., Schmidt, H., Schnur, R., Segschneider, J., Six, K. D., Stockhause, M., Timmreck, C., Wegner, J., Widmann, H., Wieners, K.-H., Claussen, M., Marotzke, J., and Stevens, B.: Climate and carbon cycle changes from 1850 to 2100 in MPI-ESM simulations for the Coupled Model Intercomparison Project phase 5, J. Adv. Model. Earth Syst., 5, 572–597, https://doi.org/10.1002/jame.20038, 2013.

Giorgi, F. and Gutowski, W. J.: Regional Dynamical Downscaling and the CORDEX Initiative, Annu. Rev. Environ. Resour., 40, 467–490, https://doi.org/10.1146/annurev-environ-102014-021217, 2015.

Gleeson, T., Moosdorf, N., Hartmann, J., and van Beek, L. P. H.: A glimpse beneath earth's surface: GLobal HYdrogeology MaPS (GLHYMPS) of permeability and porosity, Geophys. Res. Lett., 41, 3891–3898, https://doi.org/10.1002/2014GL059856, 2014.

Grasselt, René and Schüttemeyer, D., Warrach-Sagi, K., Ament, F., and Simmer, C.: Validation of TERRA-ML with discharge measurements, Meteorol. Z., 17, 763–773, https://doi.org/10.1127/0941-2948/2008/0334, 2008.

Gutowski, W. J., Giorgi, F., Timbal, B., Frigon, A., Jacob, D., Kang, H.-S., Raghavan, K., Lee, B., Lennard, C., Nikulin, G., O'Rourke, E., Rixen, M., Solman, S., Stephenson, T., and Tangang, F.: WCRP COordinated Regional Downscaling EXperiment (CORDEX): a diagnostic MIP for CMIP6, Geosci. Model Dev., 9, 4087–4095, https://doi.org/10.5194/gmd-9-4087-2016, 2016.

Hari, V., Rakovec, O., Markonis, Y., Hanel, M., and Kumar, R.: Increased future occurrences of the exceptional 2018-2019 Central European drought under global warming, Sci. Rep., 10, 12207, https://doi.org/10.1038/s41598-020-68872-9, 2020.

Hartick, C., Furusho-Percot, C., Goergen, K., and Kollet, S.: An Interannual Probabilistic Assessment of Subsurface Water Storage Over Europe Using a Fully Coupled Terrestrial Model, Water Resour. Res., 57, e2020WR027828, https://doi.org/https://doi.org/10.1029/2020WR027828, 2021.

Hartick, C., Furusho-Percot, C., Clark, M. P., and Kollet, S.: An Interannual Drought Feedback Loop Affects the Surface Energy Balance and Cloud Properties, Geophys. Res. Lett., 49, e2022GL100 924, https://doi.org/10.1029/2022GL100924, 2022.

Hawkins, E. and Sutton, R.: The Potential to Narrow Uncertainty in Regional Climate Predictions, Bull. Am. Meteorol. Soc., 90, 1095–1108, https://doi.org/10.1175/2009BAMS2607.1, 2009.

Horton, R. M., Mankin, J. S., Lesk, C., Coffel, E., and Raymond, C.: Review of Recent Advances in Research on Extreme Heat Events, Curr. Clim. Change. Rep., 2, 242–259, https://doi.org/10.1007/s40641-016-0042-x, 2016.

Iles, C. E., Vautard, R., Strachan, J., Joussaume, S., Eggen, B. R., and Hewitt, C. D.: The benefits of increasing resolution in global and regional climate simulations for European climate extremes, Geosci. Model Dev., 13, 5583–5607, https://doi.org/10.5194/gmd-13-5583-2020, 2020.

Ionita, M., Nagavciuc, V., Kumar, R., and Rakovec, O.: On the curious case of the recent decade, mid-spring precipitation deficit in central Europe, NPJ Clim. Atmos. Sci., 3, 49, https://doi.org/10.1038/s41612-020-00153-8, 2020.

Jach, L., Schwitalla, T., Branch, O., Warrach-Sagi, K., and Wulfmeyer, V.: Sensitivity of land–atmosphere coupling strength to changing atmospheric temperature and moisture over Europe, Earth Syst. Dynam., 13, 109–132, https://doi.org/10.5194/esd-13-109-2022, 2022.

Jacob, D. and Podzun, R.: Sensitivity studies with the regional climate model REMO, Meteorl. Atmos. Phys., 63, 119–129, https://doi.org/10.1007/BF01025368, 1997.

Jacob, D., Teichmann, C., Sobolowski, S., and et al.: Regional climate downscaling over Europe: perspectives from the EURO-CORDEX community, Reg. Environ. Change, 20, 51, https://doi.org/10.1007/s10113-020-01606-9, 2020.

Kautz, L.-A., Martius, O., Pfahl, S., Pinto, J. G., Ramos, A. M., Sousa, P. M., and Woollings, T.: Atmospheric blocking and weather extremes over the Euro-Atlantic sector – a review, Weather Clim. Dynam., 3, 305–336, https://doi.org/10.5194/wcd-3-305-2022, 2022.

Kendon, E. J., Jones, R. G., Kjellström, E., and Murphy, J. M.: Using and Designing GCM-RCM Ensemble Regional Climate Projections, J. Climate, 23, 6485–6503, https://doi.org/10.1175/2010JCLI3502.1, 2010.

Keune, J., Gasper, F., Goergen, K., Hense, A., Shrestha, P., Sulis, M., and Kollet, S.: Studying the influence of groundwater representations on land surface-atmosphere feedbacks during the European heat wave in 2003, J. Geophys. Res. Atmos., 121, 13 301–13 325, https://doi.org/10.1002/2016JD025426, 2016.

Knist, S., Goergen, K., Buonomo, E., Christensen, O. B., Colette, A., Cardoso, R. M., Fealy, R., Fernández, J., García-Díez, M., Jacob, D., Kartsios, S., Katragkou, E., Keuler, K., Mayer, S., van Meijgaard, E., Nikulin, G., Soares, P. M. M., Sobolowski, S., Szepszo, G., Teichmann, C., Vautard, R., Warrach-Sagi, K., Wulfmeyer, V., and Simmer, C.: Land-atmosphere coupling in EURO-CORDEX evaluation experiments, J. Geophys. Res. Atmos., 122, 79–103, https://doi.org/10.1002/2016JD025476, 2017.

Kollet, S. J. and Maxwell, R. M.: Integrated surface–groundwater flow modeling: A free-surface overland flow boundary condition in a parallel groundwater flow model, Adv. Water. Resour., 29, 945–958, https://doi.org/10.1016/j.advwatres.2005.08.006, 2006.

Kollet, S. J. and Maxwell, R. M.: Capturing the influence of groundwater dynamics on land surface processes using an integrated, distributed watershed model, Water Resour. Res., 44, W02402, https://doi.org/10.1029/2007WR006004, 2008.

Koster, R. D., Schubert, S. D., and Suarez, M. J.: Analyzing the Concurrence of Meteorological Droughts and Warm Periods, with Implications for the Determination of Evaporative Regime, J. Clim., 22, 3331–3341, https://doi.org/10.1175/2008JCLI2718.1, 2009.

Kuffour, B. N. O., Engdahl, N. B., Woodward, C. S., Condon, L. E., Kollet, S., and Maxwell, R. M.: Simulating coupled surface–subsurface flows with ParFlow v3.5.0: capabilities, applications, and ongoing development of an open-source, massively parallel, integrated hydrologic model, Geosci. Model Dev., 13, 1373–1397, https://doi.org/10.5194/gmd-13-1373-2020, 2020.

Lhotka, O. and Kyselý, J.: Characterizing joint effects of spatial extent, temperature magnitude and duration of heat waves and cold spells over Central Europe, Int. J. Climatol., 35, 1232–1244, https://doi.org/10.1002/joc.4050, 2015.

Lhotka, O., Kyselý, J., and Plavcová, E.: Evaluation of major heat waves' mechanisms in EURO-CORDEX RCMs over Central Europe, Clim. Dyn., 50, 4249–4262, https://doi.org/10.1007/s00382-017-3873-9, 2018.

Liang, X., Xie, Z., and Huang, M.: A new parameterization for surface and groundwater interactions and its impact on water budgets with the variable infiltration capacity (VIC) land surface model, J. Geophys. Res., 108, 8613, https://doi.org/https://doi.org/10.1029/2002JD003090, 2003.

Liu, X., He, B., Guo, L., Huang, L., and Chen, D.: Similarities and Differences in the Mechanisms Causing the European Summer Heatwaves in 2003, 2010, and 2018, Earth's Future, 8, e2019EF001386, https://doi.org/10.1029/2019EF001386, 2020.

Manabe, S. and Delworth, T.: The temporal variability of soil wetness and its impact on climate, Climatic Change, 16, 185–192, https://doi.org/10.1007/BF00134656, 1990.

Martínez-de la Torre, A. and Miguez-Macho, G.: Groundwater influence on soil moisture memory and land–atmosphere fluxes in the Iberian Peninsula, Hydrol. Earth Syst. Sci., 23, 4909–4932, https://doi.org/10.5194/hess-23-4909-2019, 2019.

Masson-Delmotte, V., Zhai, P., Pirani, A., Connors, S., Péan, C., Berger, S., Caud, N.and Chen, Y., Goldfarb, L., Gomis, M., Huang, M., Leitzell, K., Lonnoy, I., Matthews, J., Maycock, T., Waterfield, T., Yelekçi, O., Yu, R., and B., Z., eds.: IPCC report, Climate Change 2021: The Physical Science Basis. Contribution of Working Group I to the Sixth Assessment Report of the Intergovernmental Panel on Climate Change, Cambridge University Press, Cambridge, United Kingdom and New York, NY, USA, https://www.ipcc.ch/report/ar6/wg1/downloads/report/IPCC_AR6_WGI_FullReport.pdf, 2021.

Maxwell, R. M. and Condon, L. E.: Connections between groundwater flow and transpiration partitioning, Science, 353, 377–380, https://doi.org/10.1126/science.aaf7891, 2016.

Maxwell, R. M. and Miller, N. L.: Development of a Coupled Land Surface and Groundwater Model, J. Hydrometeorol., 6, 233–247, https://doi.org/10.1175/JHM422.1, 2005.

Maxwell, R. M., Chow, F. K., and Kollet, S. J.: The groundwater–land-surface–atmosphere connection: Soil moisture effects on the atmospheric boundary layer in fully-coupled simulations, Adv. Water Resour., 30, 2447–2466, https://doi.org/10.1016/j.advwatres.2007.05.018, 2007.

Mearns, L. O., Lettenmaier, D. P., and McGinnis, S.: Uses of Results of Regional Climate Model Experiments for Impacts and Adaptation Studies: the Example of NARCCAP, Curr. Clim. Change Rep., 1, 1–9, https://doi.org/10.1007/s40641-015-0004-8, 2015.

Miralles, D. G., van den Berg, M. J., Teuling, A. J., and de Jeu, R. A. M.: Soil moisture-temperature coupling: A multiscale observational analysis, Geophys. Res. Lett., 39, L21707, https://doi.org/10.1029/2012GL053703, 2012.

Molina, M. O., Sánchez, E., and Gutiérrez, C.: Future heat waves over the Mediterranean from an Euro-CORDEX regional climate model ensemble, Sci. Rep., 10, 8801, https://doi.org/10.1038/s41598-020-65663-0, 2020.

Mu, M., Pitman, A. J., De Kauwe, M. G., Ukkola, A. M., and Ge, J.: How do groundwater dynamics influence heatwaves in southeast Australia?, Weather Clim. Extrem., 37, 100 479, https://doi.org/10.1016/j.wace.2022.100479, 2022.

Myhre, G., Alterskjær, K., Stjern, C. W., Hodnebrog, Ø., Marelle, L., Samset, B. H., Sillmann, J., Schaller, N., Fischer, E., Schulz, M., and Stohl, A.: Frequency of extreme precipitation increases extensively with event rareness under global warming, Sci. Rep., 9, 16063, https://doi.org/10.1038/s41598-019-52277-4, 2019.

Nairn, J. R. and Fawcett, R. J. B.: The excess heat factor: a metric for heatwave intensity and its use in classifying heatwave severity, Int. J. Environ. Res. Public Health, 12, 227–253, https://doi.org/10.3390/ijerph120100227, 2014.

Niu, G.-Y., Yang, Z.-L., Dickinson, R. E., Gulden, L. E., and Su, H.: Development of a simple groundwater model for use in climate models and evaluation with Gravity Recovery and Climate Experiment data, J. Geophys. Res. Atmos., 112, D07103, https://doi.org/10.1029/2006JD007522, 2007.

Oleson, K., Dai, Y., Bonan, G. B., Bosilovichm, M., Dickinson, R., Dirmeyer, P., and et al.: Technical Description of the Community Land Model (CLM) (No. NCAR/TN-461+STR), Tech. rep., University Corporation for Atmospheric Research, https://doi.org/10.5065/D6N877R0, 2004.

Oleson, K. W., Niu, G.-Y., Yang, Z.-L., Lawrence, D. M., Thornton, P. E., Lawrence, P. J., Stöckli, R., Dickinson, R. E., Bonan, G. B., Levis, S., Dai, A., and Qian, T.: Improvements to the Community Land Model and their impact on the hydrological cycle, J. Geophys. Res. Biogeosci., 113, G01021, https://doi.org/10.1029/2007JG000563, 2008.

Pal, J. S. and Eltahir, E. A. B.: Pathways Relating Soil Moisture Conditions to Future Summer Rainfall within a Model of the Land–Atmosphere System, J. Climate, 14, 1227–1242, https://doi.org/https://doi.org/10.1175/1520-0442(2001)014<1227:PRSMCT>2.0.CO;2, 2001.

Perkins, S. E. and Alexander, L. V.: On the Measurement of Heat Waves, J. Clim., 26, 4500–4517, https://doi.org/10.1175/JCLI-D-12-00383.1, 2013.

Plavcová, E. and Kyselý, J.: Overly persistent circulation in climate models contributes to overestimated frequency and duration of heat waves and cold spells, Clim. Dyn., 46, 2805–2820, https://doi.org/10.1007/s00382-015-2733-8, 2016.

Pothapakula, P. K., Primo, C., Sørland, S., and Ahrens, B.: The synergistic impact of ENSO and IOD on Indian summer monsoon rainfall in observations and climate simulations – an information theory perspective, Earth Syst. Dynam., 11, 903–923, https://doi.org/10.5194/esd-11-903-2020, 2020.

Prein, A. F., Gobiet, A., Truhetz, H., Keuler, K., Goergen, K., Teichmann, C., Fox Maule, C., van Meijgaard, E., Déqué, M., Nikulin, G., Vautard, R., Colette, A., Kjellström, E., and Jacob, D.: Precipitation in the EURO-CORDEX 0.11° and 0.44° simulations: high resolution, high benefits?, Clim. Dyn., 46, 383–412, https://doi.org/10.1007/s00382-015-2589-y, 2016.

Rockel, B., Will, A., and Hense, A.: The Regional Climate Model COSMO-CLM (CCLM), Meteorol. Z., 17, 347–348, https://doi.org/10.1127/0941-2948/2008/0309, 2008.

Rummukainen, M.: Added value in regional climate modeling, WIREs Clim. Change, 7, 145–159, https://doi.org/10.1002/wcc.378, 2016.

Russo, S., Sillmann, J., and Fischer, E. M.: Top ten European heatwaves since 1950 and their occurrence in the coming decades, Environ. Res. Lett., 10, 124003, https://doi.org/10.1088/1748-9326/10/12/124003, 2015.

Schlemmer, L., Schär, C., Lüthi, D., and Strebel, L.: A Groundwater and Runoff Formulation for Weather and Climate Models, J. Adv. Model. Earth Syst., 10, 1809–1832, https://doi.org/10.1029/2017MS001260, 2018.

Seneviratne, S. I., Lüthi, D., Litschi, M., and Schär, C.: Land–atmosphere coupling and climate change in Europe, Nature, 443, 205–209, https://doi.org/10.1038/nature05095, 2006.

Seneviratne, S. I., Corti, T., Davin, E. L., Hirschi, M., Jaeger, E. B., Lehner, I., Orlowsky, B., and Teuling, A. J.: Investigating soil moisture–climate interactions in a changing climate: A review, Earth-Sci. Rev., 99, 125–161, https://doi.org/10.1016/j.earscirev.2010.02.004, 2010.

Shrestha, P., Sulis, M., Masbou, M., Kollet, S., and Simmer, C.: A Scale-Consistent Terrestrial Systems Modeling Platform Based on COSMO, CLM, and ParFlow, Mon. Weather Rev., 142, 3466–3483, https://doi.org/10.1175/MWR-D-14-00029.1, 2014.

Song, Y. M., Wang, Z. F., Qi, L. L., and Huang, A. N.: Soil Moisture Memory and Its Effect on the Surface Water and Heat Fluxes on Seasonal and Interannual Time Scales, J. Geophys. Res. Atmos., 124, 10 730–10 741, https://doi.org/10.1029/2019JD030893, 2019.

Sørland, S. L., Schär, C., Lüthi, D., and Kjellström, E.: Bias patterns and climate change signals in GCM-RCM model chains, Environ. Res. Lett., 13, 074017, https://doi.org/10.1088/1748-9326/aacc77, 2018.

Stegehuis, A. I., Vogel, M. M., Vautard, R., Ciais, P., Teuling, A. J., and Seneviratne, S. I.: Early Summer Soil Moisture Contribution to Western European Summer Warming, J. Geophys. Res. Atmos., 126, e2021JD034646, https://doi.org/10.1029/2021JD034646, 2021.

Stott, P. A., Stone, D. A., and Allen, M. R.: Human contribution to the European heatwave of 2003, Nature, 432, 610–614, https://doi.org/10.1038/nature03089, 2004.

Sulikowska, A. and Wypych, A.: Summer temperature extremes in Europe: how does the definition affect the results?, Theor. Appl. Climatol., 141, 19–30, https://doi.org/10.1007/s00704-020-03166-8, 2020.

Taylor, K. E., Stouffer, R. J., and Meehl, G. A.: An Overview of CMIP5 and the Experiment Design, Bull. Am. Meteorol. Soc., 93, 485–498, https://doi.org/10.1175/BAMS-D-11-00094.1, 2012.

Teuling, A. J., Uijlenhoet, R., van den Hurk, B., and Seneviratne, S. I.: Parameter Sensitivity in LSMs: An Analysis Using Stochastic Soil Moisture Models and ELDAS Soil Parameters, J. Hydrometeor., 10, 751–765, https://doi.org/10.1175/2008JHM1033.1, 2009.

Tomczyk, A. M. and Bednorz, E.: Heat waves in Central Europe and their circulation conditions, Int. J. Climatol., 36, 770–782, https://doi.org/10.1002/joc.4381, 2016.

Torma, C., Giorgi, F., and Coppola, E.: Added value of regional climate modeling over areas characterized by complex terrain—Precipitation over the Alps, J. Geophys. Res. Atmos., 120, 3957–3972, https://doi.org/https://doi.org/10.1002/2014JD022781, 2015.

Valcke, S.: The OASIS3 coupler: a European climate modelling community software, Geosci. Model Dev., 6, 373–388, https://doi.org/10.5194/gmd-6-373-2013, 2013.

Vautard, R., Yiou, P., D'Andrea, F., de Noblet, N., Viovy, N., Cassou, C., Polcher, J., Ciais, P., Kageyama, M., and Fan, Y.: Summertime European heat and drought waves induced by wintertime Mediterranean rainfall deficit, Geophys. Res. Lett., 34, L07711, https://doi.org/10.1029/2006GL028001, 2007.

Vautard, R., Gobiet, A., Jacob, D., and et al.: The simulation of European heat waves from an ensemble of regional climate models within the EURO-CORDEX project, Clim. Dyn., 41, 2555–2575, https://doi.org/10.1007/s00382-013-1714-z, 2013a.

Vautard, R., Noël, T., Li, L., Vrac, M., Martin, E., Dandin, P., Cattiaux, J., and Joussaume, S.: Climate variability and trends in downscaled high-resolution simulations and projections over Metropolitan France, Clim. Dyn., 41, 1419–1437, https://doi.org/10.1007/s00382-012-1621-8, 2013b.

Vautard, R., Kadygrov, N., Iles, C., Boberg, F., Buonomo, E., Bülow, K., Coppola, E., Corre, L., van Meijgaard, E., Nogherotto, R., Sandstad, M., Schwingshackl, C., Somot, S., Aalbers, E., Christensen, O. B., Ciarlo, J. M., Demory, M.-E., Giorgi, F., Jacob, D., Jones, R. G., Keuler, K., Kjellström, E., Lenderink, G., Levavasseur, G., Nikulin, G., Sillmann, J., Solidoro, C., Sørland, S. L., Steger, C., Teichmann, C., Warrach-Sagi, K., and Wulfmeyer, V.: Evaluation of the Large EURO-CORDEX Regional Climate Model Ensemble, J. Geophys. Res. Atmos., 126, e2019JD032 344, https://doi.org/10.1029/2019JD032344, 2021.

Vogel, M. M., Zscheischler, J., and Seneviratne, S. I.: Varying soil moisture–atmosphere feedbacks explain divergent temperature extremes and precipitation projections in central Europe, Earth Syst. Dyn., 9, 1107–1125, https://doi.org/10.5194/esd-9-1107-2018, 2018.

Vogt, J., Soille, P., De Jager, A., Rimaviciute, E., Mehl, W., Foisneau, S., Bodis, K., Dusart, J., Paracchini, M., Haastrup, P., and Bamps, C.: A pan-European River and Catchment Database, JRC Reference Report, Joint Research Centre, Institute for Environment and Sustainability, https://doi.org/10.2788/35907, 2007.

Voldoire, A., Sanchez-Gomez, E., Salas y Mélia, D., and et al: The CNRM-CM5.1 global climate model: description and basic evaluation, Clim. Dyn., 40, 2091–2121, https://doi.org/10.1007/s00382-011-1259-y, 2013.

Yang, L., Sun, G., Zhi, L., and Zhao, J.: Negative soil moisture-precipitation feedback in dry and wet regions, Sci Rep, 8, 4026, https://doi.org/10.1038/s41598-018-22394-7, 2018.

Yeh, P. J.-F. and Eltahir, E. A. B.: Representation of Water Table Dynamics in a Land Surface Scheme. Part I: Model Development, J. Climate, 18, 1861–1880, https://doi.org/10.1175/JCLI3330.1, 2005.

Yin, C., Yang, Y., Chen, X., Yue, X., Liu, Y., and Xin, Y.: Changes in global heat waves and its socioeconomic exposure in a warmer future, Clim. Risk Manag., 38, 100 459, https://doi.org/10.1016/j.crm.2022.100459, 2022.

Yule, E. L., Hegerl, G., Schurer, A., and Hawkins, E.: Using early extremes to place the 2022 UK heat waves into historical context, Atmos. Sci. Lett., e1159, https://doi.org/10.1002/asl.1159, 2023.

Zhang, R., Sun, C., Zhu, J., Zhang, R., and Li, W.: Increased European heat waves in recent decades in response to shrinking Arctic sea ice and Eurasian snow cover, npj Clim. Atmos. Sci., 3, 7, https://doi.org/10.1038/s41612-020-0110-8, 2020.

Zhang, X., Hegerl, G., Zwiers, F., and Kenyon, J.: Avoiding Inhomogeneity in Percentile-Based Indices of Temperature Extremes, J. Clim., 38, 1641–1651, https://doi.org/10.1175/JCLI3366.1, 2005.

Zhang, X., Alexander, L., Hegerl, G. C., Jones, P., Tank, A. K., Peterson, T. C., Trewin, B., and Zwiers, F. W.: Indices for monitoring changes in extremes based on daily temperature and precipitation data, WIREs Clim. Change, 2, 851–870, https://doi.org/10.1002/wcc.147, 2011.